Spring 2018

De-embedding method comparisons and physics based circuit model for high frequency D-probe

Yuan Chen

Recommended Citation

DE-EMBEDDING METHOD COMPARISONS AND

PHYSICS BASED CIRCUIT MODEL FOR HIGH FREQUENCY D-PROBE

by

YUAN CHEN

A THESIS

Presented to the Faculty of the Graduate School of the

MISSOURI UNIVERSITY OF SCIENCE AND TECHNOLOGY

In Partial Fulfillment of the Requirements for the Degree

MASTER OF SCIENCE IN ELECTRICAL ENGINEERING

2018

Approved by

Dr. James Drewniak, Advisor
Dr. Jun Fan
Dr. Victor Khilkevich

ABSTRACT

In section 1, the procedures of 1X-Reflect smart fixture de-embedding (SFD), 1-port auto fixture removal (AFR), and 2X-Thru SFD are compared from various perspectives: test fixture design, the de-embedding procedure, and de-embedded results. The accuracy of fixture characterization and the de-embedded result is the key figure of merit (FOM) in each de-embedding method. Full wave models are built to evaluate the FOM of the three methods, by comparing the scattering parameters (S-parameters) and time domain reflectometer (TDR). A test coupon for measuring USB-C cables is adopted to serve as a manufactured validation purpose.

In section 2, a physics-based circuit model for a novel differential probe without a nearby ground pin is built up to 20GHz. First, the SFD method is used to obtain the S-parameter of a differential probe in a full wave model to validate the effectiveness of this method. Second, real measurements are made to obtain the S-parameter of a differential probe. Furthermore, the one-to-one corresponding circuit model has been built to understand the physics of probes. A layout for the advance interconnect test tool (AITT) demo board is then designed to test probe characteristics and AITT software. Finally, the SFD method is applied to de-embed the test fixtures, and material information is extracted based on the de-embedded results.

ACKNOWLEDGMENTS

Foremost, I would like to express my sincere gratitude to my advisor Dr. Drewniak for the continuous support of my Master study and research, for his patience, motivation, enthusiasm, and immense knowledge. It is a great honor to work under his supervision.

I also would like to thank my committee member, Dr. Fan and Dr. Khikevich. Their door to their office are always open whenever I ran into a trouble spot or had a question about my research or writing.

I also feel grateful to Bichen Chen, who is my mentor during the research period and provided me a lot of help. I also want to thank Han Deng, Qian Wang, Jiayi He, Yansheng Wang, Ying Cao, Kyoungchoul Koo, who helped me a lot in my research and life in Rolla. Also my thanks go to all of the other faculty members and my fellow lab mates in the EMC group of Missouri S&T. I am happy to work with you.

Finally, I must express my very profound gratitude to my parents and my husband, for providing me with unfailing support and continuous encouragement throughout my years of study and through the process of researching and writing this thesis.

TABLE OF CONTENTS

LIST OF ILLUSTRATIONS

LIST OF TABLES

1. INTRODUCTION

Due to measurement limitations, devices under test (DUTs) commonly require test fixtures to be inserted between the DUT and pre-requisite interface of the equipment for measurement. However, the discontinuities introduced by test fixtures are usually an unavoidable challenge for engineers. Therefore, de-embedding is a necessary procedure to obtain the scattering parameters (S-parameters) of a DUT [1]. As a consequence, an accurate and cost-effective de-embedding procedure has become critical in the industrial field. Manufacturing variations are inevitable in nearly all test vehicles, which creates major inaccuracies in de-embedding results.

The classic and prevailing calibration and de-embedding methodologies include: thru-reflect-line (TRL) [2], short-open-load (SOL) [3], thru-line de-embedding, 2X-Thru and 1X-Reflect SFD (from EMCLAB, Missouri S&T) [4]-[6], and 2X-Thru auto fixture removal (AFR) (from Keysight). These de-embedding methodologies have different theories and algorithms, and each has its own advantages and drawbacks. The figure of merit (FOM) of de-embedding is the accuracy of fixture characterization and de-embedded results. The ease of measurement and designing space of the test fixture are also important for de-embedding. Moreover, signal integrity applications such as electrical performance quantification, material extraction [7]-[10], and crosstalk mitigation [11]-[12] are highly dependent on de-embedding. This paper compares 1X-Reflect SFD, 1-port AFR, and 2X-Thru SFD, with an emphasis on the calibration patterns and test fixture design requirements, fixture characterization, and a comparison of the de-embedded results. The 1X-Reflect and 2X-Thru SFD methodologies were developed in EMCLAB, Missouri S&T.

Microprobes play an important role in high-frequency measurement, including printed circuit board (PCB) level, radio frequency (RF) [13]-[18], and other signal integrity applications. In general, a commercial microprobe has three transitions: 1) test system to probe interface, 2) RF transition inside the probe, and 3) probe tips to DUT. Three types of microprobe are common, including differential signal (SS) probes, signal-ground-signal (SGS) probes, and ground-signal-signal-ground (GSSG) probes [19]-[20]. The distance between probe tips (pitch size) is a key factor in probe performance at higher frequency, as a result of smaller measurement parasitics. Compared with GSSG probes, SS probes only require two signal pads when performing measurements, which significantly shrinks the probe landing space and is especially suitable for most on die measurements and applications where space is minimal. In addition, removing nearby GND pins is more convenient for bare boards, populated boards, and boards with solder bumps when performing measurements.

Accurate electrical characterization of high-speed test fixtures (such as cables, interconnects, and lead-in traces) is a critical step in any de-embedding procedure. Using the known electrical characterization of such test fixtures, de-embedding can be used to rigorously remove the effects of these fixtures, thus exposing the true performance of the DUT. In order to remove the unexpected element performance and extract the true DUT performance, the SFD tool for removing fixture artifacts is used.

The Advanced Interconnect Test Tool (AITT) is a powerful and user-friendly commercial software. The tool includes four key features: VNA control, a de-embedding tool, an analysis tool, and applications; for instance, Intel Delta-L+ and USB type C .Delta-L methodology accommodates the different focuses and needs at different stages

of PCB. AITT tool provides three methods for different cases, to be chosen by the customer. The methodologies and functions of AITT were developed by EMCLAB, Missouri S&T.

2. DE-EMBEDDING PROCEDURE COMPARISON

There are a few popular calibration methods which are widely used today, Like TRL, 2X-Thru SFD method, AFR method. Because a vector network requires that a measurement calibration be performed before error-corrected measurement can be made. For two-port measurements, the calibration algorithm used will be determine the appropriate calibration kit, known either as SOLT or TRL.

Another two port calibration type utilizes a minimum of three standards to define the calibrated reference plane. The measured parameters of the Thru, Reflect, and Line standards in a TRL calibration kit provides the same information as a SOLT calibration via a different algorithm.

The TRL involves certain restrictions, which include: 1) characteristic impedances and propagation constants among the thru and line standards are required to be identical; 2) broad-frequency coverage requires multiple line standards; and 3) the interconnects in the thru, reflect, and line standards are assumed to be identical. The drawbacks of SOLT-like methods are: 1) poor low-frequency behaviors; and 2) uncontrollable parasitics for manufacturing standards. In addition, the complexity of the TRL and SOLT families is much larger than that of the novel 1X-Reflect and 2X-Thru methods. The proposed method has less limitation, and provide high accuracy compared with other calibration methods.

Table 2.1 presents general conclusions on required calibration patterns and the pros and cons of de-embedding methodologies.

Table 2.1. Comparison of different calibration /de-embedding methods.

	Calibration standards	Pros	Cons
SOLT	Short Open Load Thru	Classic method.	1. Low accuracy at high frequency. 2. Expensive calibration kit. 3. Port match for DUT and cal-kit.
TRL	Thru Reflection Line(s)	Suitable for DUTs in PCBs or packages.	1. Time consuming. 2. A few assumptions. 3. Not cost effective.
2X SFD	2X Thru	1. Only 2X thru pattern is needed. 2. Smallest number of standards is needed.	1. Symmetry in the 2x Thru is assumed. 2. Discontinuities in the 2x Thru and DUT are assumed to be identical. 3. Minimum spacing between discontinuities in the 2x Thru is needed
1X-Reflect SFD	1X open or 1X short	1. Only 1X open or 1X short is needed. 2. Most cost effective.	1. Discontinuities in 1X open/short are assumed to be identical.

2.1. DE-EMBEDDING METHOD

A de-embedding method is applied to remove the unwanted fixture effects. The first step is to convert the S-parameter to a T-parameter, so that the T matrix can be utilized to perform de-embedding. The de-embedding is a mathematic calculation in the transfer scatting parameters, as shown in Eq. (2.1).

$$[T_{DUT}] = [T_{1X\_left}]^{-1} \times [T_{Total}] \times [T_{1X\_right}]^{-1} \tag{2.1}$$

$$\begin{bmatrix} T_{11} & T_{12} \\ T_{21} & T_{22} \end{bmatrix} = \frac{1}{S_{21}} \begin{bmatrix} S_{12}S_{21} - S_{11}S_{22} & S_{11} \\ -S_{22} & 1 \end{bmatrix} \tag{2.2}$$

The T-parameters are converted from S-parameters as defined in Eq. (2.2). The S-parameter acquisition procedure is fixture characterization, which is calculated through different algorithms in 1X-Reflect, 2X-Thru SFD, and 1-port AFR. This chapter elaborates on fixture characterization in these three methods from the perspective of calibration pattern requirements, test fixture designing, and assumptions.

2.1.1. 2X-thru SFD. In the 2X-Thru SFD method, the S-parameter in the frequency domain and TDR waveform in the time domain are all used in the 2X-fixture. In the real measurement procedure, the coaxial ports are extended to match the port of VNA. Figure 2.1 illustrates the 2X-Thru SFD calibration patterns and workflow. In order to obtain the S-parameter of 1X left and 1X right, a 2X fixture is proposed to be designed symmetrically and passively. Meanwhile, in the fixture characterization procedure of 2X-Thru SFD the S_{11} left and right fixtures are calculated from the time domain, while the S_{21} and S_{22} fixtures are obtained from the wave peeling algorithm. In conclusion, inputs for the 2X-Thru SFD algorithm are the S-parameter of the total structure and 2X fixture, and the output is the S-parameter of the DUT.
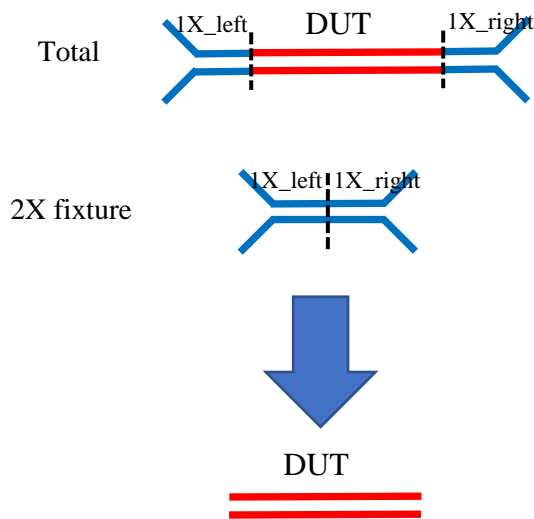
Figure 2.1. Design of 2X-Thru SFD basic model.

In 2X-Thru SFD method, asymmetric compensation and fixture error correction are implemented to enforce the accuracy of the results. The asymmetry and errors originate from inevitable manufacturing variations, which are assumed as small perturbations as opposed to drastic differences. Subsequently, sensitivity analysis [21] and de-embedding error bounds [22] are implemented to illustrate the correctness of the de-embedded results. Due to these limitations and assumptions, a more cost-effective and simple de-embedding procedure is proposed, namely 1X-Reflect SFD.

2.1.1. 1X-Reflect SFD. This proposed de-embedding method only requires two calibration patterns to obtain the DUT S-parameter, as depicted in Figure 2.2. In this design, 1X left and 1X right are not necessarily symmetric, and are characterized separately. However, if 1X left and 1X right are symmetric then only one 1X fixture is designed. Compared with the 2X SFD method, 1X left open and 1X right open replace the 2X fixture, in this method, less limitation will be required. As a consequence, the

limitations associated with asymmetry and manufacturing variations are eliminated in 1X-Reflect SFD.
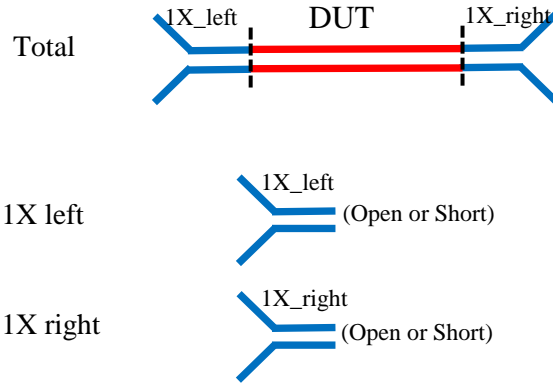
Figure 2.2. Design of 1X-Reflect SFD basic model.

The electrical performance of the 1X fixture is constructed first by the time domain method, then transferred into the frequency domain. For instance, if we obtain the S-parameter of 1X left open, we can then obtain the open TDR curve in the time domain. Some of the same characteristics are shared for open/short/load, so subsequently it is possible to obtain the short/load TDR curve. The SOL algorithm is used to acquire the S-parameter of 1X-Thru. Finally, the de-embedding workflow can be implemented as discussed previously. Figure 2.3 shows the workflow of the 1X-Reflect SFD method.
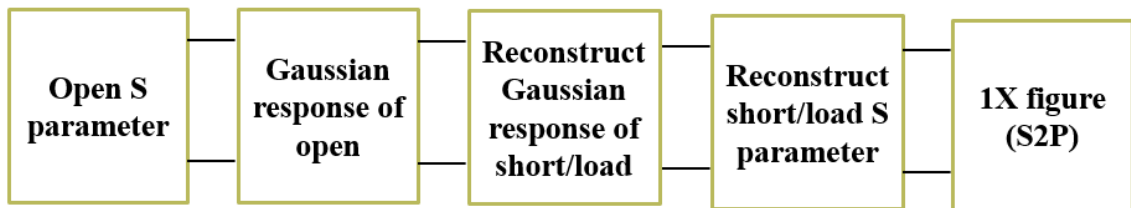
Figure 2.3. Workflow of the 1X-Reflect SFD method.

2.2. SIMULATION AND MEASUREMENT FOR VALIDATION

In order to validate the proposed 1X-Reflect SFD method, ADS circuit model, full wave models, and real measurements are used. The results of the proposed de-embedding method are then compared with 2X-Thru SFD and 1X AFR.

2.2.1. Validation Through Circuit Models. In this ADS circuit, the open circuit is present with inductance and the ideal transmission line. Based on the 1X-Reflect SFD method algorithm, the 1X open circuit can be reconstructed to become the 1X-Thru circuit, as shown in the red box in Figure 2.4.
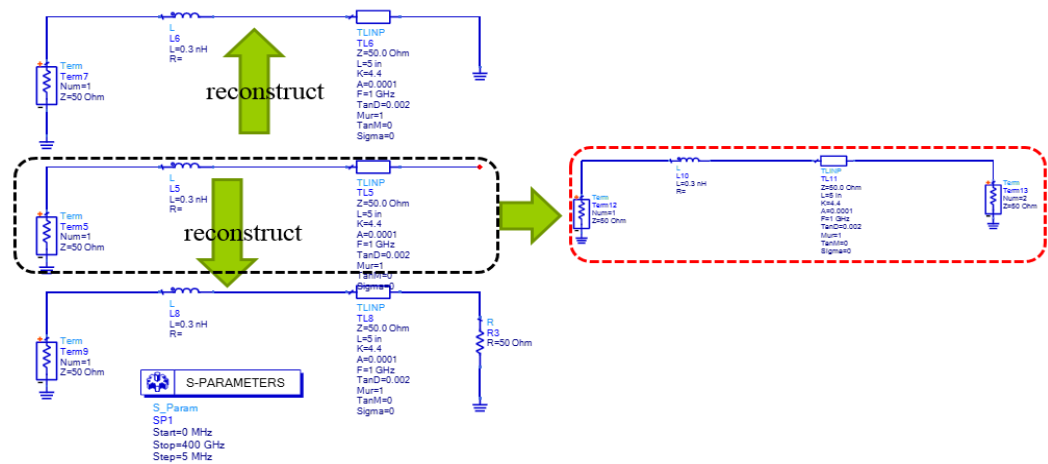
Figure 2.4 ADS circuit to validate 1X-Reflect SFD method.

Figure 2.5 compares the results of the reconstructed S-parameter and the golden standard. The latter is directly obtained from the 1X-Thru ADS circuit, and exhibits a very good match up to 50GHz. The ADS circuit validates that the proposed 1X-Reflect SFD method could have a great agreement with gold standard in the simple circuit.
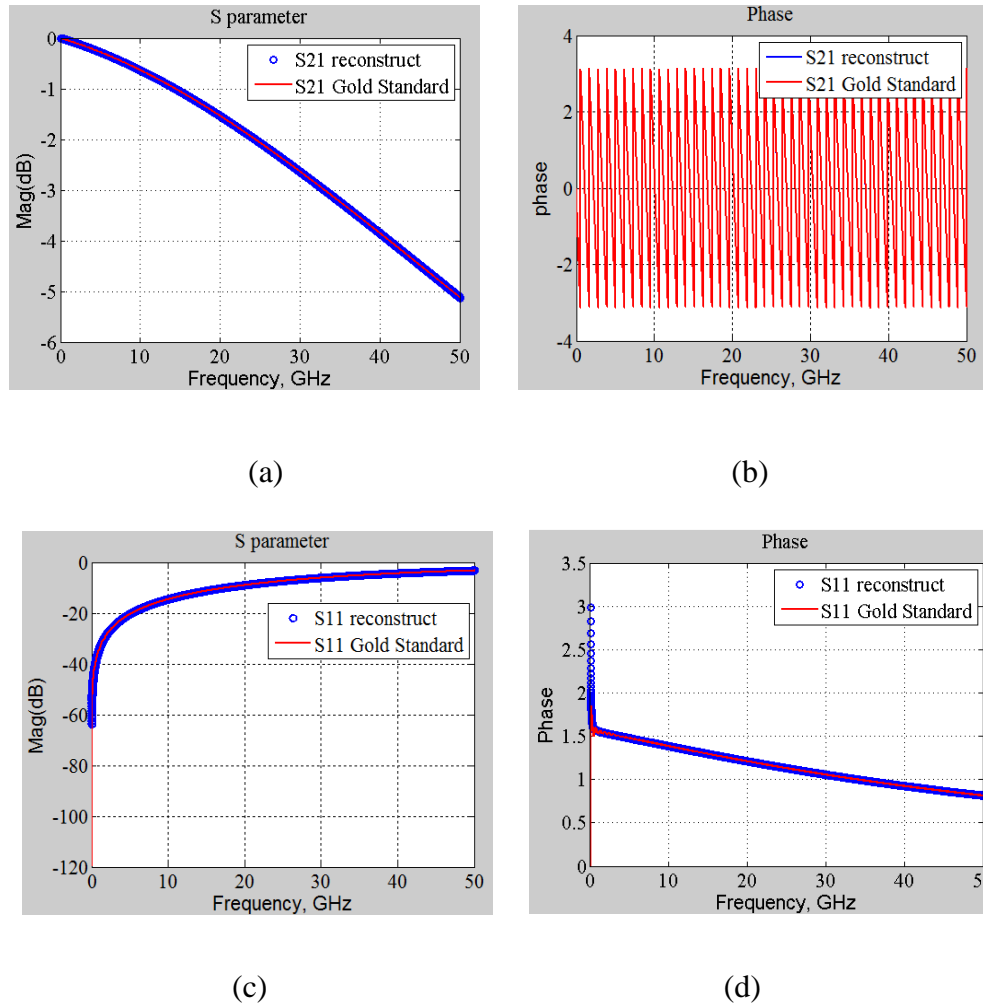
Figure 2.5. Comparison of the reconstructed S-parameter with the golden standard.

2.2.1. Validation Through Full Wave Models. In this part, two full wave models are built in CST to conduct the FOM comparison of 1X-Reflect and 2X-Thru SFD, in addition to AFR. The simulated test fixtures serve as a golden standard.

Figure 2.6 shows the full wave model of 1X open and detailed information about the transition from coax to single-ended stripline. A four-layer board design is used in the simulation model. The relative epsilon is 3.7 and El.tand is 0.02 in the material setting. Furthermore, the transition part has been optimized [23]-[24], which includes 50ohm

characteristic impedance, via design, anti-pad size, and signal pad size. The trace length is 500mil and the total thickness is 63mil. The simulation results for the S-parameter and TDR are shown in Figure 2.6. In the TDR curve, a small dip of approximately 47 ohm can be seen at 2.08ns, corresponding to the transition. The 1X open is designed for the 1X-Reflect SFD and 1-port AFR methods.

(a)

$R_{antipad} = 24mil$

$H = 62mil$ $R_{via} = 7.5mil$ $H_{core} = 39mil$

$R_{pad} = 12.5mil$

(b)

(c)

(d)
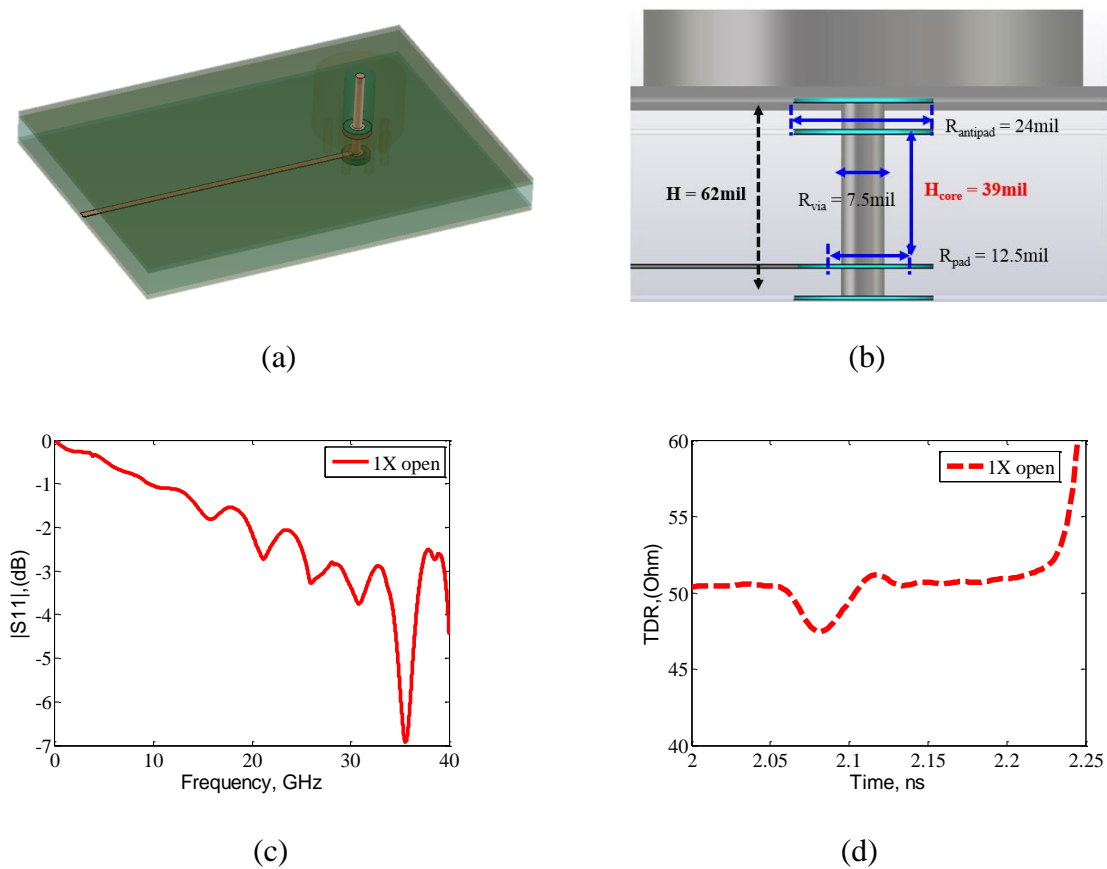
Figure 2.6. 1X open full wave model and simulation results.

Due to the requirement of the 2X-Thru SFD method, the full wave model is designed to be symmetrical and reciprocal. Figure 2.6 shows the full wave model of 2X-Thru, which is a 1-inch single-ended trace with the same interconnection geometry as 1X

open. Waveguide ports are set in the coax part. Two dips are visible in the TDR curve

due to two transition parts in the 2X-Thru design, and the characteristic impedance is also

close to 50 Ω.

(a)

(b)

(c)
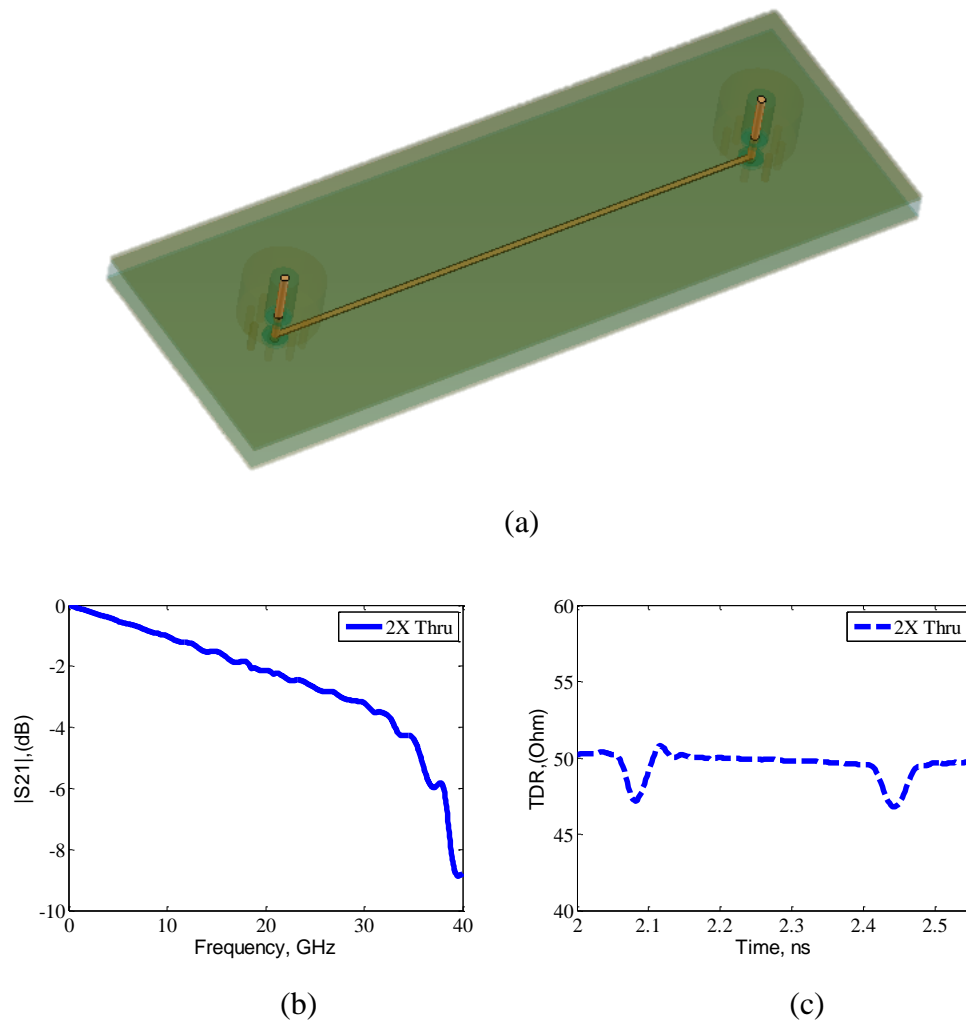
Figure 2.7. 2X-Thru full wave model and simulation results.(a) shows the full wave
model in the CST;(b) shows the magnitude of insertion loss and (c) shows the TDR result
for 2X Thru.

The S-parameter of 1X-Thru is required in the de-embedding procedure, as

discussed in the previous sections. Figure 2.8 depicts the comparison of 1X-Thru directly

from the CST model, 1X-Reflect SFD, and 1-port AFD and 2X-Thru SFD. Figure 2.8

illustrates the insertion loss magnitude, phase, return loss, and TDR comparison,

respectively. The comparison results show good agreement for the different de-

embedding methods up to 40GHz. The proposed 1X-Reflect method has a comparable

results as other de-embeding methods.

(a) (b)

(c) (d)
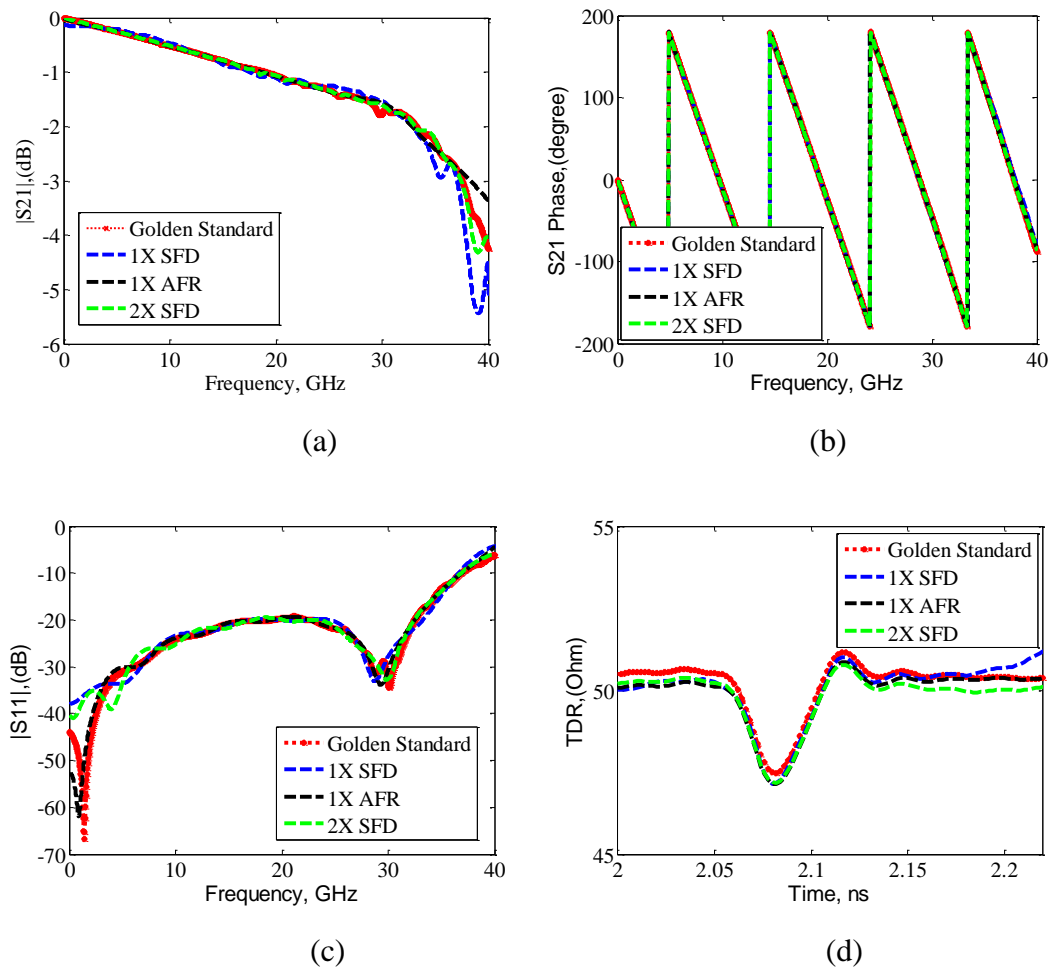
Figure 2.8. Comparison results of different calibration methods, including insertion loss magnitude(a), phase(b), return loss magnitude(c) and TDR(d) from Golden Standard (red line), 1X Thru SFD (blue line) method, 1 port AFR (black line) and 2X SFD (green line),respectively.

2.2.1. Validation Through Measurement. This part discusses real measurement cases and validates the proposed 1X-Reflect SFD method, before presenting a comparison with 1-port AFR and 2X-Thru SFD.

The USB type C cable is widely used to plug in peripheral devices, such as printers, smartphones, or external hard devices. Since the USB-C cable cannot directly connect VNA to perform measurement, a port extension is necessary when measuring. Figure 2.9 shows the USB-C cable with left and right fixtures on the PCB board.

The 1m USB-C cable is the DUT embedded in the fixtures. In order to obtain the S-parameter of the DUT, de-embedding is necessary. The top half of PCB is for 1X-Reflect SFD and 1-port AFR, while the bottom half comprises calibration patterns for 2X-Thru SFD. The connectors, indicated by blue rectangles in Figure 2.9, are the connected ports with VNA. The PCB of this type of test vehicle has 2X-Thru calibration on board, as shown in the yellow box in Figure 2.9. However, for the 1X-Reflect SFD and 1-port AFR, no extra calibration pattern is needed. The test fixtures are reused in the total measurement by connection to the USB-C cables.
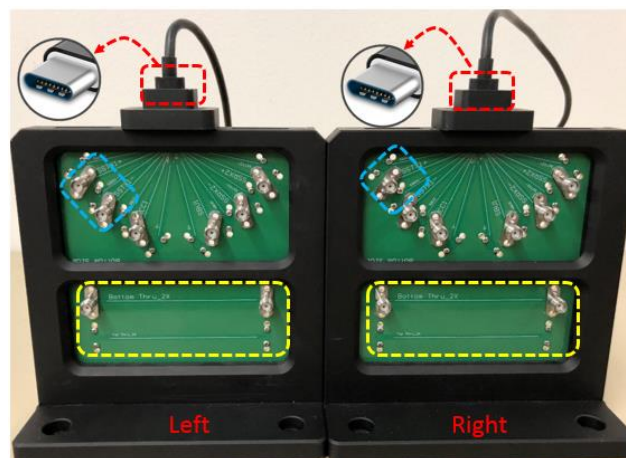
Figure 2.9. USB - C cable with left and right fixture.

S-parameter measurement is performed by Keysight PNA N5245, with a frequency range of 10MHz~20GHz. Prior to measurement, the cable is removed using e-cal. For measurement of 1X open, The 1X fixtures could be open directly. The experimental setup is shown in Figure 2.10.

(a)   (b)
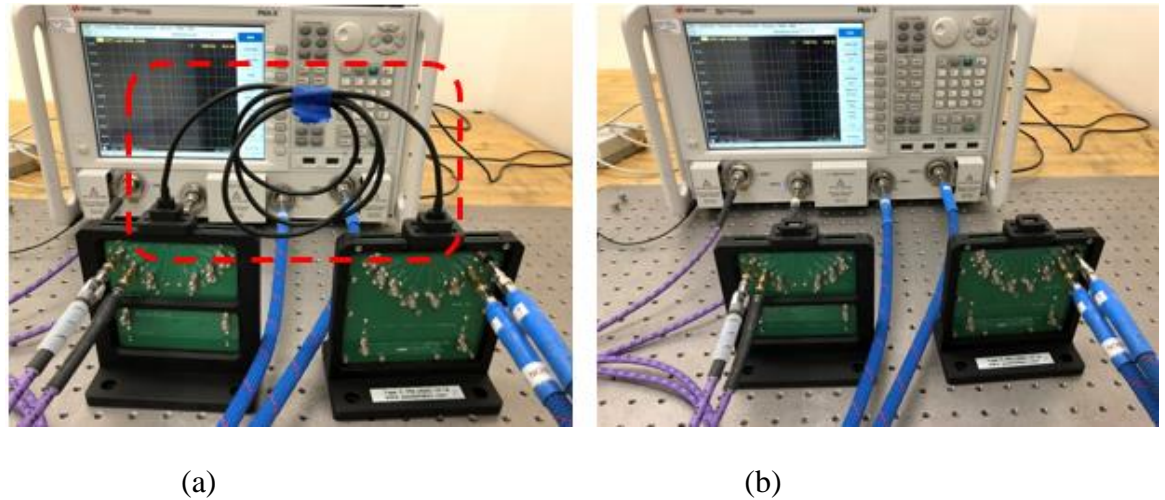
Figure 2.10. S-parameter measurement setup for total structure and 1X open.

Figure 2.11 shows the measurement results for the total structure, 1X left open, and 1X right open. The TDR indicates that the designed differential characteristic impedance of the USB-C cable is close to 90 Ohm. (a) shows the magnitude of insertion loss and (b) shows the TDR for total structure. The total delay time for total structure is about 13 ns. The discontinuity on the TDR curve is corresponding to the connection part for 1X fixture and USB-C cable. (c) and (d) show the magnitude of return loss and TDR for 1X right/left. The red line represents the results from 1X left fixture, and blue line represents the results from 1X right fixture. Because 1X on the left board and right board are different, they need two 2X Thru to do de-embedding. And the delay time for 1X left

and 1X right are about 2.7 ns. Also, when doing the measurement, 1X on the test board
is open, so the TDR shows to be infinite.

(a)

(b)

(c)

(d)
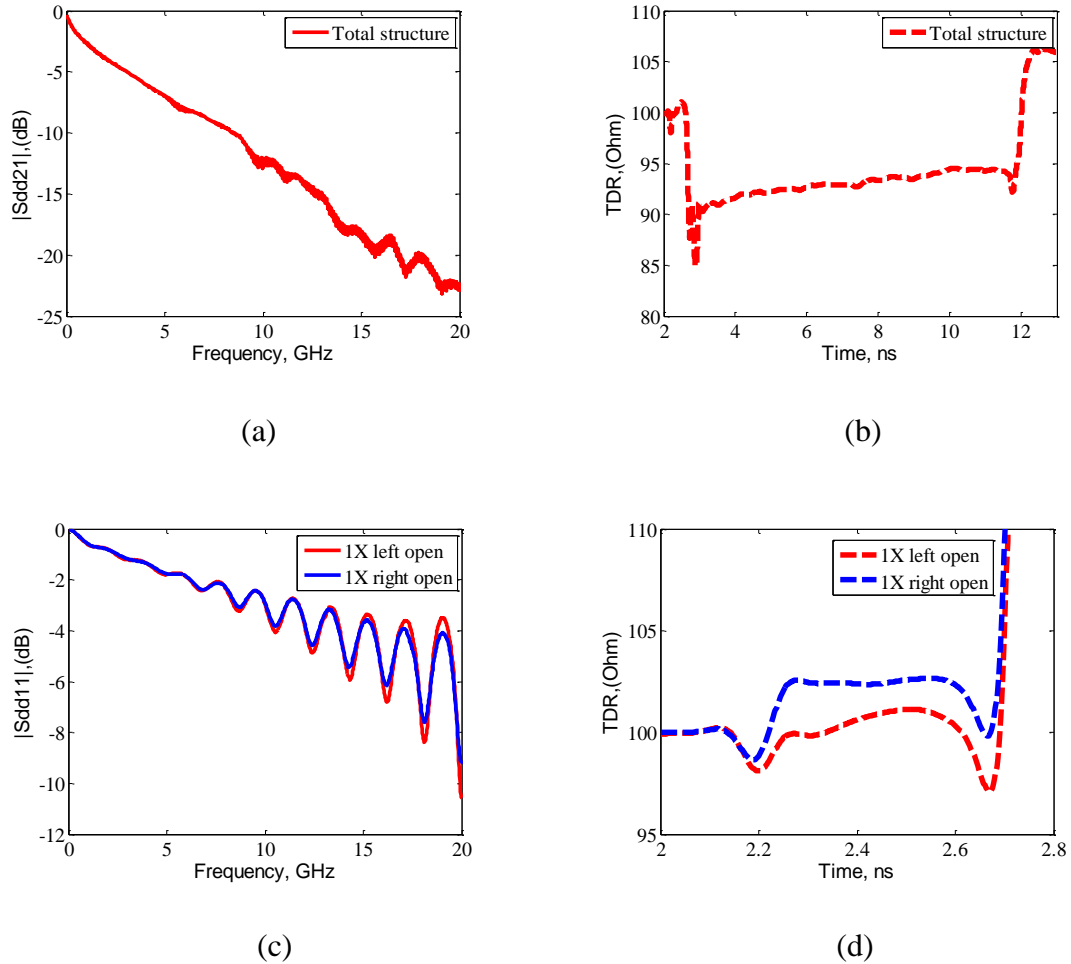
Figure 2.11. Measurement results for total structure and 1X open.

Figure 2.12 represents the de-embedded results of DUT by using 1X-Reflect SFD,
1-port AFR, and 2X-Thru SFD, including insertion loss magnitude, return loss
magnitude, and TDR comparison, respectively. The 1X-Reflect and 2X-Thru have more
consistent de-embedded results compared with 1X AFR. The designed differential
characteristic impedance of the USB-C cable is 90ohm. As indicated in the following

TDR plot, 1X-Reflect SFD and 2X-Thru SFD exhibit better characteristic impedance agreement with the specification. One possible reason for the 1X AFR TDR measurement mismatch is the 1X AFR algorithm for the open S-parameter. In the simulation case, it is open without parasitic and both 1X-Reflect de-embedding algorithms could obtain 1X-Thru. However, it is difficult to obtain the perfect open in the measurement.

(a)

(b)

(c)
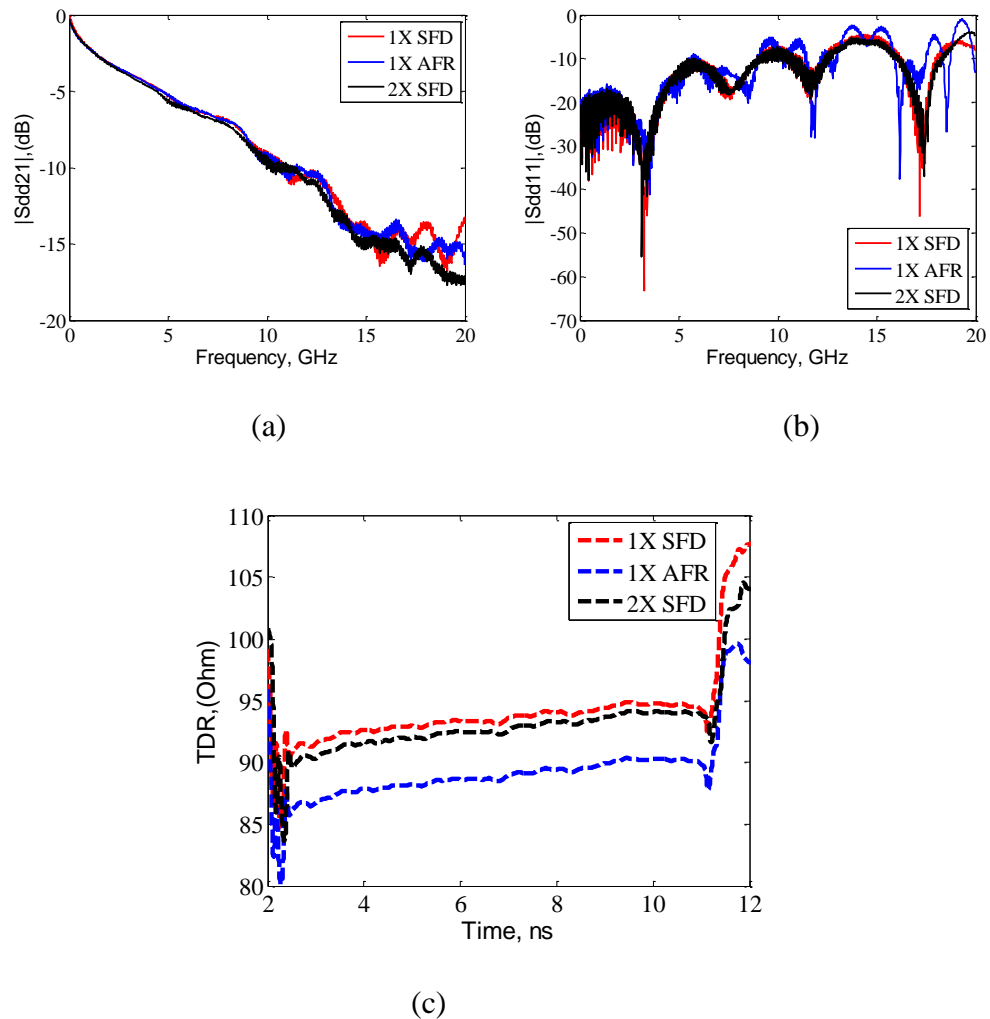
Figure 2.12. Comparison results in real measurement for three methods; (a) insertion loss magnitude,(b) return loss magnitude and (c)TDR by using 1X SFD,1X AFR and 2X SFD, respectively.

2.2.1. GUI FOR SFD. The commercial software for SFD de-embedding is completed, and the graphical user interface (GUI) is shown in Figure 2.13. In this software, users only need to load the S-parameter of the total structure and 2X-Thru/1X short/1X open to obtain the DUT S-parameter.
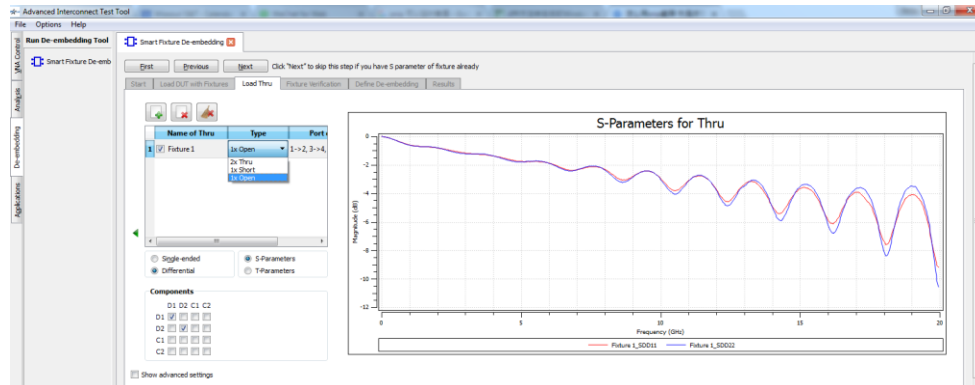
Figure 2.13. GUI for 1X-Reflect SFD and 2X-Thru SFD.

This software is developed by MST EMCLABlab, which is friendly to users with very good accuracy. The software could be used to extract large-bandwidth network parameters for modeling of interconnects, such as circuit board traces and vias, connectors, IC packets, and cables.

3. PHYSICS BASED CIRCUIT MODEL FOR 1MM PITCH D-PROBE

In this section, 2X-Thru SFD method will be used to extract the S parameter of DUT in full wave simulation and real measurement. Also, based on the understanding of current distribution on probe tips, the physics based equivalent circuit model has been built and compared with the real measurement results.

3.1. 1MM PITCH D-PROBE

Figure 3.1 shows the 1mm pitch D-probe and a detailed view of the probe tips, which can operate up to 20GHz. The D-probe has strong beryllium copper (BeCu) tips that are mechanically very robust, and suitable for landing on rough or uneven surfaces such as solder balls and BGAs. The D-probe only requires only two signal pins for signal integrity measurements on differential signals. In addition, removing the landing pads for GND reduces the space required for landing the probe; this is suitable for applications where space is limited, such as on-die applications. However, despite the robust mechanical design and ease of landing while maintaining superior differential electrical performance during measurement, the common-mode information of a DUT cannot be measured due to a lack of ground contact.
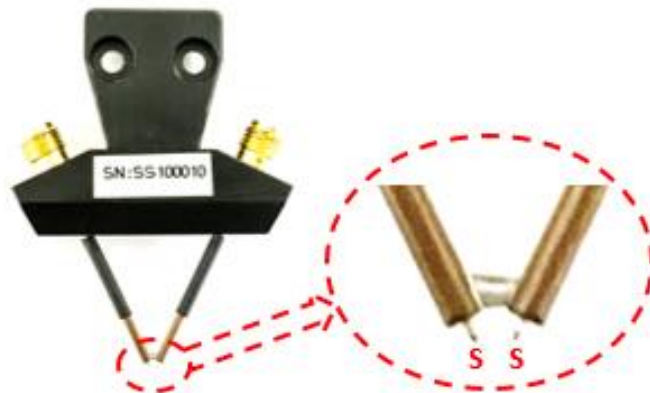
Figure 3.1. 1mm pitch D-probe with a detailed view of tips.

In Figure 3.2, a 3D CAD model shows the complete detail of the D-probe geometry, together with a metal base that facilitates probe alignment and landing for the special geometry that is used for material parameter extraction. The metal base with guide-pins ensures repeatable and easy probe landing.
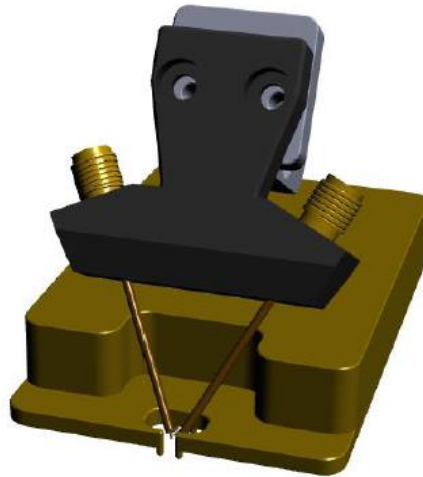
Figure 3.2. 3D model for D-probe with a mechanical base holder.

D-probes are powerful and widely used in the industry, and the user experience of a D-probe is similar to that of the microprobe. The Precision Positioner TP300 allows an engineer to easily switch between the D-probe (with the TP300-PA Probe Adapter) and microprobe. Some key features of the 1mm pitch D-probe are summarized below:

- High bandwidth: DC to 20GHz;

- Low insertion loss: <3dB @20GHz;

- Signal-signal only: accurate S-parameter and TDR measurements without the need of nearby ground pads;

- Ruggedness: strong enough for direct probing of uneven solder bumps;

- High repeatability: no moving parts;

- Applications: measurements for DDR memory, flex PCB, and PCB characterization.

3.2. SFD WORKFLOW AND CHEETAH 8 DESIGN

In order to obtain the S-parameter of a 1mm pitch D-probe, the 2X-Thru SFD method is used. The SFD method will be discussed to obtain the S parameter for DUT.

3.2.1. 2X-Thru SFD Method Used to Extract S Parameter of D Probe. Figure 3.3 shows a one-to-one comparison of the 2X-Thru SFD flow and 3D full wave model. Because of the requirements of the 2X-Thru SFD method. According to the 2X-Thru algorithm, the user could obtain the S-parameter of left-1X and right-1X, and subsequently obtain the S-parameter of the probe. The relative epsilon is 4.3 and El.tand is 0.02 in the material setting. The transition part has been optimized, which includes 100ohm differential characteristic impedance, U-shaped pad, a transition part from the signal-ended trace to differential trace, and a transition part from the connector to PCB.
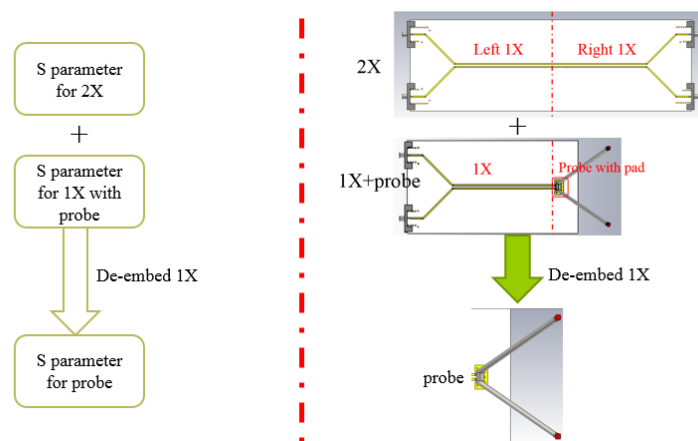
Figure 3.3. One-to-one comparison of the 2X-Thru SFD workflow and 3D model.

In addition, the SFD method procedure must ensure that the break point uses transverse electromagnetic (TEM) mode; TEM is a mode of propagation whereby the electric and magnetic field lines are restricted to directions transverse to the direction of propagation. TEM waves are characterized by $E_z=H_z=0$, and TEM waves can exist when two or more conductors are present. Plane waves are examples of TEM waves, since no field components exist in the direction of propagation. Quasi-TEM wave mode exists in a microstrip, where the term "quasi" implies that this wave resembles a TEM wave.

Figure 3.4 shows the top view of 1X with probe, where the left side is differential microstrip, which is the TEM mode region, and the right side is a U-shaped pad with probe, which is non-TEM mode region. Therefore, the distance between the U-shaped pad and microstrip must be determined and d should be as short as possible at 20GHz, as marked in Figure 3.4.
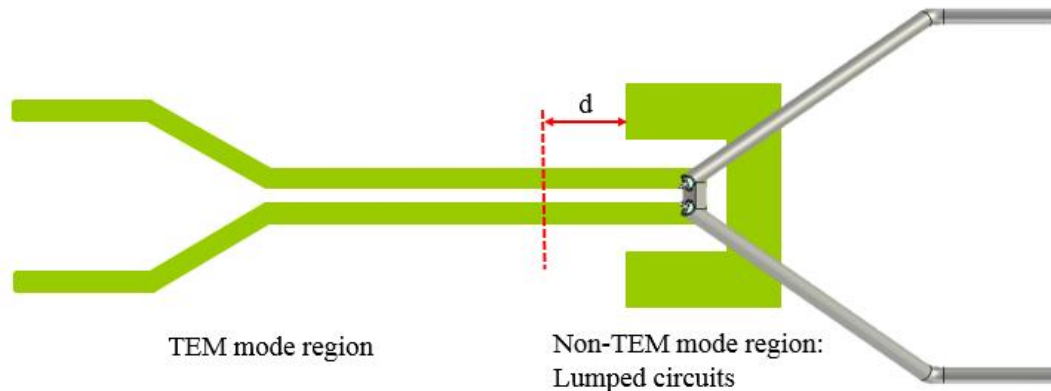
Figure 3.4. Top view of 1X with probe.

In order to obtain the E field value from a CST model, a field monitor at 20GHz should be added. After simulation, the E field values are shown in the 3D results part; the

results can then be combined to attain differential E fields of the longitudinal and transverse direction. Figure 3.5 shows the results of $|E_{Transverse}|$ and $E_{Longitudinal}/|E_{Transverse}|$. According to the plots, the magnitude of the E transverse field is constant, and the ratio of $|E_{Longitudinal}|$ and $|E_{Transverse}|$ is less than 0.01 when distance exceeds 60mil. This implies that there is nearly no mode to the direction of propagation. Finally, the shortest distance is 60mil, where the break point is in TEM mode.

(a)   (b)
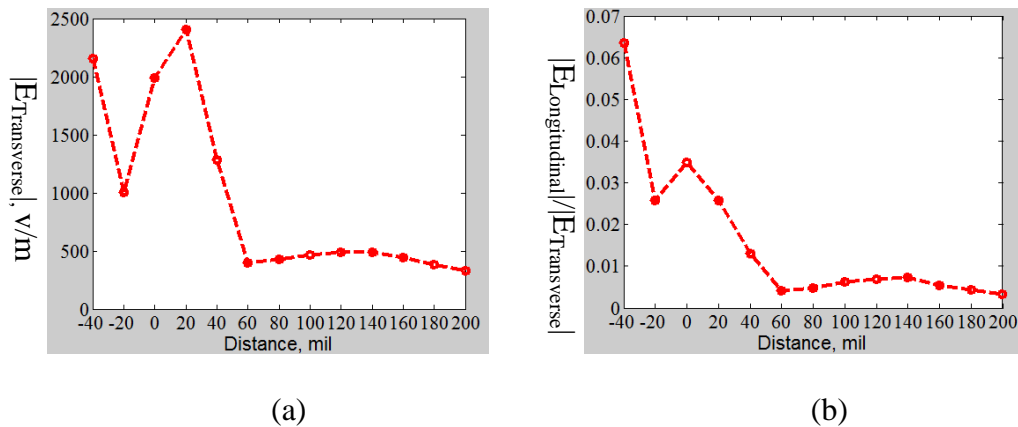
Figure 3.5. The magnitude of $|E_{Transverse}|$ and ratio of $|E_{Longitudinal}|$ and $|E_{Transverse}|$.

In order to make the transition part from the 1mm pitch probe and PCB, a number of full wave models are built. Based on the measured dimensions, a full wave simulation model is developed for the 1mm pitch differential probe. Figure 3.6 (a) shows the whole view of simulation model of differential probe and probe tip, and (b) shows the details view of probe tips. The distance of probe tips is 1mm which is exactly the same as real product. The angler of probe coax is 52 degree. The dielectric used in the simulation model for coax is Teflon, with a permittivity of 2.1. The simulation frequency ranges from 10MHz to 20GHz. To ensure the accuracy of the developed simulation model for

the differential probe, the simulation result comparison are validated in the reference paper [7].

(a)   (b)
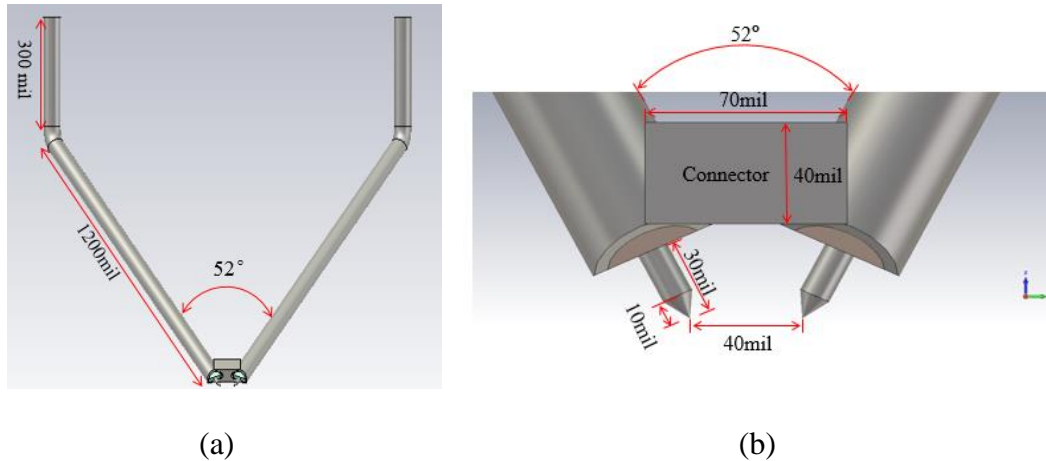
Figure 3.6. The full wave simulation model of 1mm pitch D probe.

The entire transition structure consists of two coax connectors, a single-ended trace, a 1,300mil differential trace, a U-shaped pad, and a 1mm pitch probe, as shown in Figure 3.7. The simulation model for the microstrip is FR4, with a permittivity of 4.3. The differential trace width is 15mil and the center-to-center trace space is 40mil. The thickness of the first layer is 9.0mil, and its characteristic impedance is optimized to be 100ohm [25]-[26]. The shape of the unified U-shaped pad is rectangular, with dimensions 106 mil*196 mil, while the rectangular pad size is 20mil*25mil. Four waveguide ports are set, and the boundary condition is open space. The frequency range is 10MHz to 20GHz. (b) and (c) shows the detail view of probe tips and U shape pad. The shape of unified U shape pad is rectangular with dimension 106 mil*196 mil. And the rectangular pad size is 20mil*25mil. The distance between two signal pads is 40mil, which matches the distance in the real product.

(a) (b) (c)
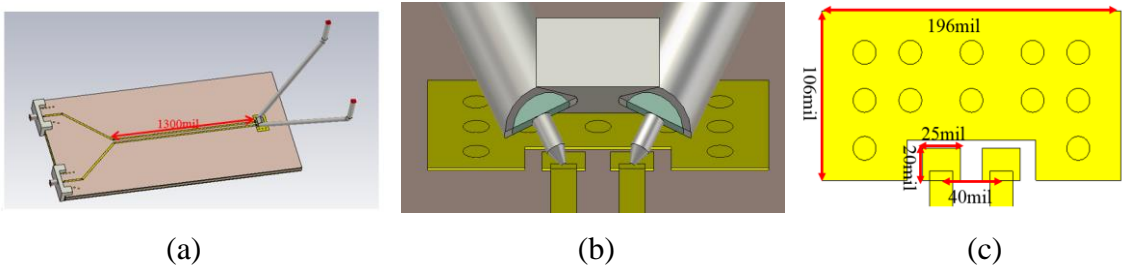
Figure 3.7. Whole view and details view of 1X with 1mm pitch probe.

The full wave simulation result for 1X with 1mm pitch probe is shown in Figure 3.8. The magnitude of insertion loss is -5dB at 20GHz with a linear scale. Meanwhile, the magnitude of return loss is less than -10dB, and the envelope period is about 2.5GHz. The insertion loss is 5dB larger than the return loss, which meets the SFD requirement.

(a) (b)
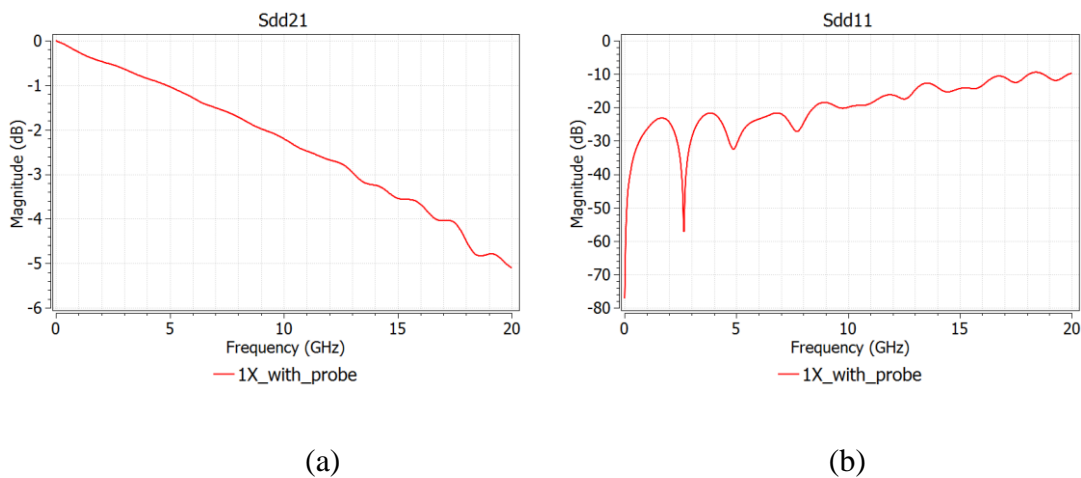
Figure 3.8. Simulation results for 1X with probe in the full wave model.

The full wave model and simulation result for 2X is shown in Figure 3.9. Four waveguide ports are set at the end of the connector. The length of the differential microstrip is 2,480mil. As the previous section discussed, there are 60 mil differential

microstrip traces left in the DUT structure. Therefore, the differential traces length is 2480. So trace length for 1X is 1240. Every other condition is kept the same as in the full wave model of 1X with probe. The simulation results show that the total insertion loss is -8dB at 20GHz with a linear scale, while the return loss is less than -15dB. In the next section, the model of DUT only will be built and its simulation results will be compared with SFD results.
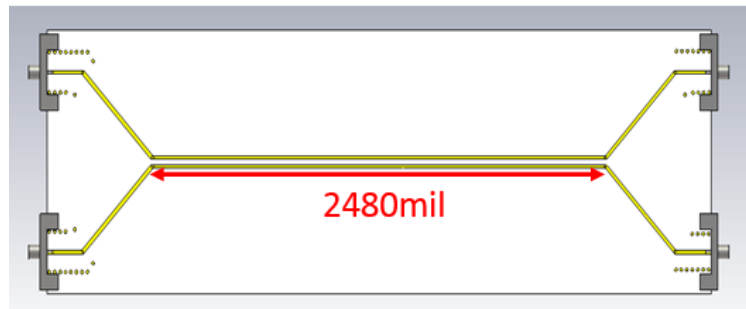
(a)
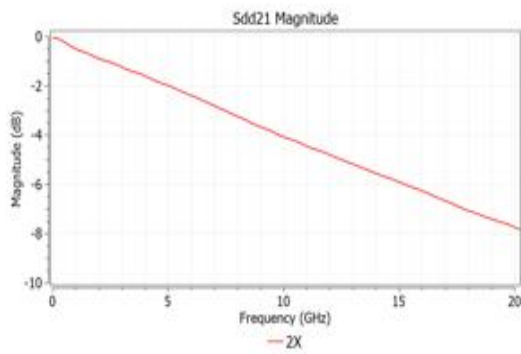
(b)
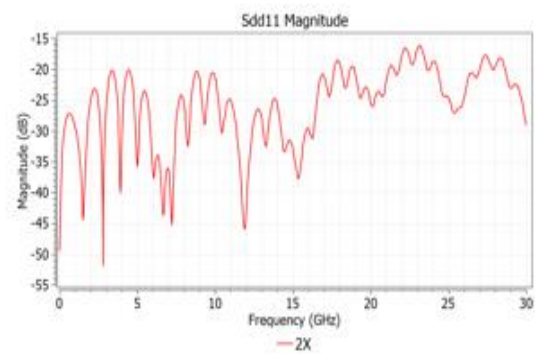
(c)

Figure 3.9. Full wave model and simulation results for 2X-Thru fixture.

In order to validate the accuracy of the 2X-Thru SFD method to extract the probe S-parameter, the other choice is to perform simulation for the probe with a U-shaped pad

only, and to compare this with the SFD results. The full wave model for a probe with U-shaped pad is shown in Figure 3.10. Two waveguide ports and two discrete ports are set. Every other condition is kept the same as in the full wave model of 1X with probe. However, under real conditions it is impossible to make a direct measurement, due to the VNA port limitation. Hence, this method can verify and predict the SFD method in the real measurement; this method is called direct simulation.
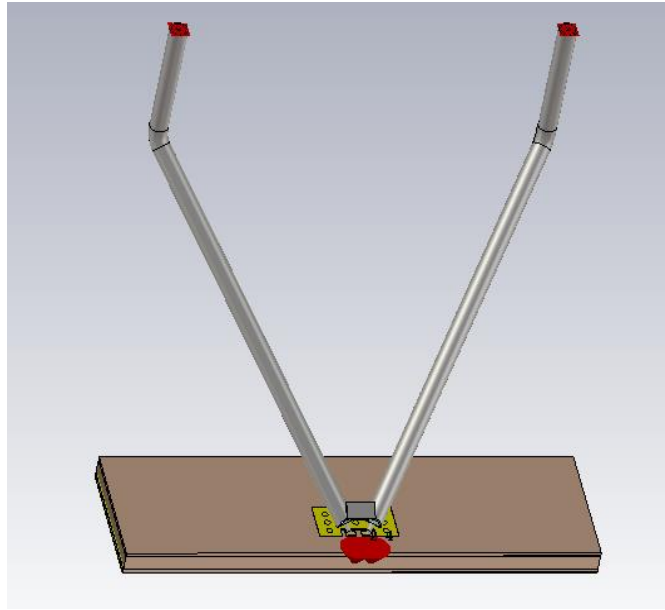
Figure 3.10. Full wave model of probe with U-shaped pad.

Figure 3.11 compares simulation results of the SFD method and direct simulation, which include the magnitude and phase of insertion loss, and the magnitude of return loss. The results show good agreement, implying that the SFD method is able to extract the probe S-parameter with a U-shaped pad in the real measurement. The total loss for DUT at 20GHz is less than 2dB based on two different methods. This probe has a very good performance in the RF application.

(a)	(b)	(c)
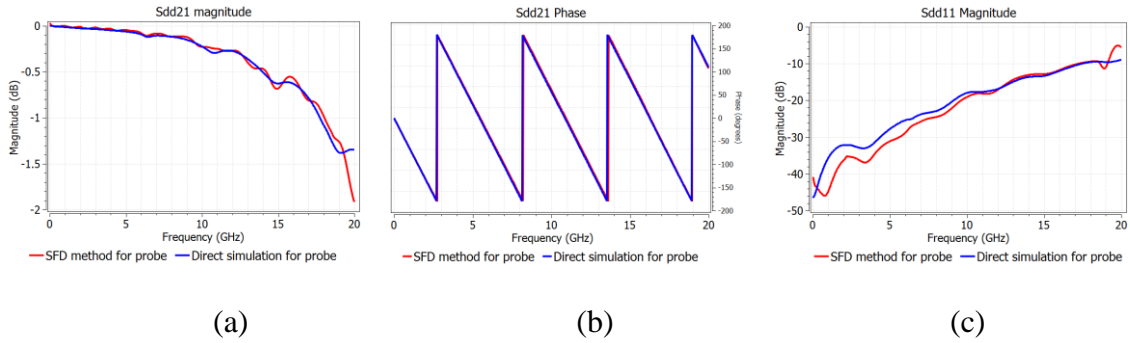
Figure 3.11. Simulation results comparison for SFD method and direct simulation.

Layout and TDR Measurement for Cheetah 8. In this section, the layout for Cheetah 8 will be provided. And the details view of Cheetah 8 will be shown. Previous simulation show the SFD method possible to extract the S parameter of probe. The next step is to do the layout and validate it in the measurement. And our physics based circuit model will be built based on the measurement results. Compared to the simulation results, the real measurement results are more accurate to build the physics model. The simulation model can help us to forecast the measurement results. Therefore, the value from physics based circuit model need to follow the real measurement results. All parameters in the physics based model will match the measurement results. Figure 3.12 shows the Cheetah 8 layout, with an overview of the top side (a), a detailed view for 2X-Thru (b), detailed view of 1X with U-shaped pad, and a zoomed-in view of the U-shaped pad (d). The total size of Cheetah 8 is 3.5inch*6.5inch, with the same details as the 3D full wave model. According to the manufacturer datasheet, the PCB material is FR4 with a relative permittivity of 4.4. The total thickness for the board is 66 mil. The thickness for each layer is about 10 mil, 40mil and 10mil. The thickness for copper is 1.3mil.
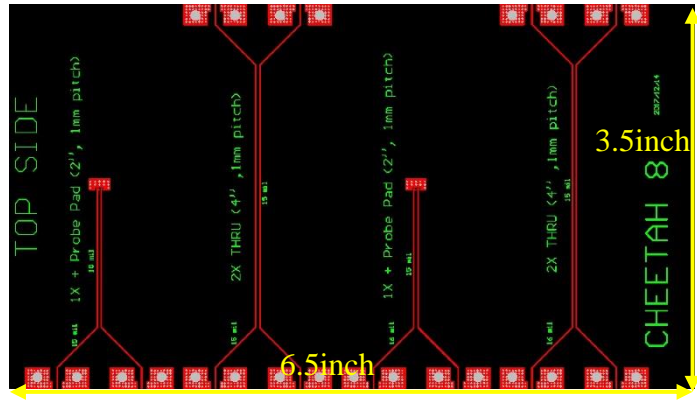
(a)
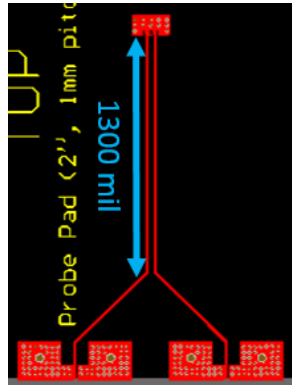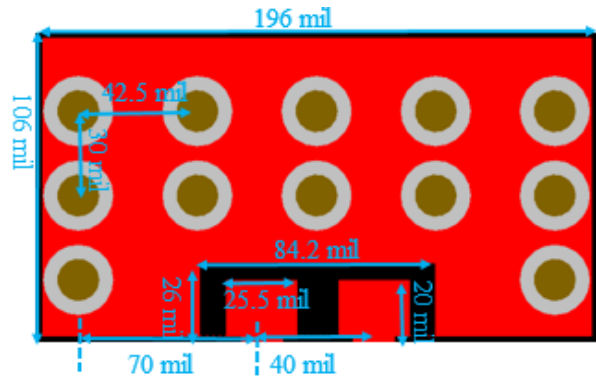
(b)   (c)   (d)

Figure 3.12. Layout review for Cheetah 8.

TDR is a methodology for measuring impedance and discontinuities in the time domain, while TDR measures reflections along a conductor. In order to measure those reflections, TDR transmits an incident signal onto the conductor and listens for its reflections. If the conductor is of a uniform impedance and is properly terminated, then there will be no reflections and the remaining incident signal is absorbed at the far-end by the termination. Alternatively, if impedance variations do exist, then some of the incident

signal is reflected back to the source. Based on the reflections, the TDR curve shows

the details of impedance variations and provides a guide.

For the differential TDR measurement, two ports are needed to connect with two

cables on the same side, and the TDR instruments should be set to the differential model.

Based on the TDR measurement results, it is straightforward to obtain probe and PCB

discontinuity information in the time domain. The total view of Cheetah 8 is shown in

Figure 3.13. This test board includes two parts: 1X with probe pad and 2X Thru.

Figure 3.13. Top view of test board.

The setup for TDR measurement are shown in Figure 3.14 (a) and the details view

of probe with U shape pad are shown in Figure 3.14 (b). The TDR measurement result is

shown in Figure 3.14 (c). In the TDR curve, the bump represents the inductor, and

integration of the area indicates that the inductance value is 1.1nH. Meanwhile, the dip

represents the capacitor, and integration of the area returns a capacitance value of 15fF.

The period from 12.8ns to 13.2ns represents the coax for the D-probe, and its

characteristic impedance is roughly 102ohm. The delay time is 0.5ns. The period from

13.2ns to 13.8ns represents 1X through, and the characteristic impedance is roughly 95ohm. The delay time is 0.5ns.
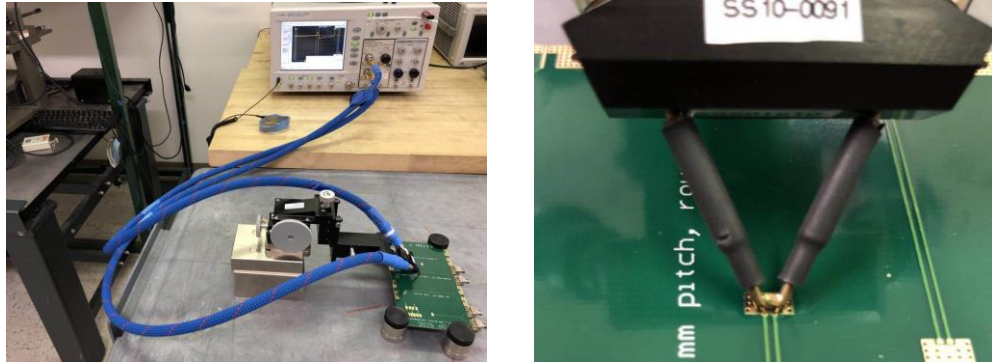
(a)   (b)
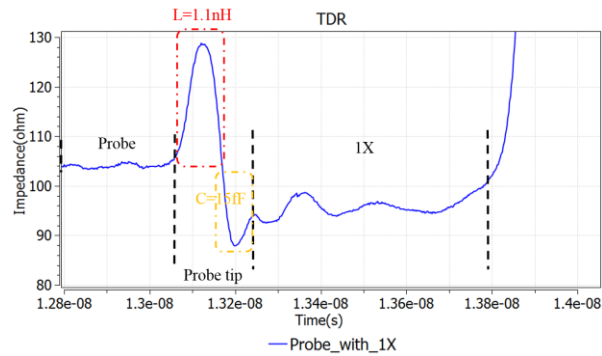
(c)

Figure 3.14. TDR measurement setup and result for 1X with probe.

3.2.1. S Parameter Measurement for Cheetah 8. S-parameters are a complex matrix that show reflection/transmission characteristics (amplitude/phase) in the frequency domain. With amplitude and phase information, it is possible to quantify the reflection and transmission characteristics of devices. Some of the most commonly measured terms are scalar in nature. For instance, the return loss is the scalar

measurement of reflection, while impedance results from a vector reflection measurement. Meanwhile, the Smith chart maps rectilinear impedance plane onto a polar plane. On the Smith chart, the vertical lines on the rectilinear plane that indicate values of constant resistance map to circles, and horizontal lines that indicate values of constant reactance map to arcs. Z_0 maps to the exact center of the chart. This is useful for evaluation of the impedance matching network.

In today's high- speed digital applications, differential signaling is used increasingly widely and commonly. This is due to the advantages of differential signaling, which are summarized below:

1. High noise immunity: differential signaling can cancel common mode noise;

2. Suitable for very low signal level application; since differential signals act as a reference for each other rather than the normal GND;

3. No net return current on the reference for pure differential signaling;

4. Switching timing can be more precisely set with differential signals than signal end noise;

5. Low EMI cancels out magnetic field (complementary current).

Of course, disadvantages also exist for differential signaling. Because of the double trace, it requires more area to route. Additionally, the differential trace length needs strictly control to be the same. Otherwise, potential issues may arise. The S parameter setup for 1X with D probe shows in Figure 3.15, which is performed with Keysight PNA N5245. This instrument includes 4 ports and with the coax connector diameter is 2.4mm. The connector in the probe is 3.5mm, so it needs two adaptor to make them connected.
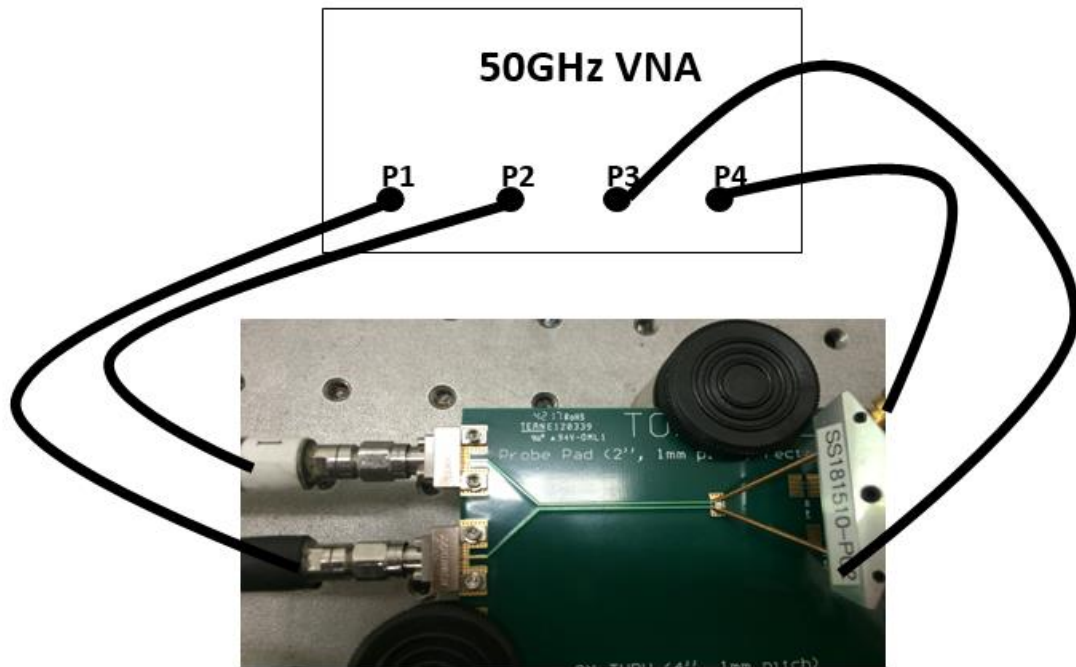
Figure 3.15. S parameter measurement setup for1X with probe.

A four-port VNA is used to carry out the measurement. Before measuring, SOLT calibration is performed to move the reference plane of measurement from the ports of VNA to the ends of cables. Following calibration, the differential probe and adaptor are connected with precision cables, and then landed onto the signal pad. The frequency ranges from 10MHz to 20GHz. The measurement results are shown in Figure 3.16. (a); (b) shows the magnitude and phase of insertion loss; (c) shows the magnitude of return loss; (d) shows the TDR for 1X with probe. The left side from TDR curve start from probe part. And the bump at 2.6ns is responded to the probe tips to U shape pads. The characteristic impedance of differential trace is about 97ohm. This part include 1X fixture, 1mm pitch probe and precious adaptors.
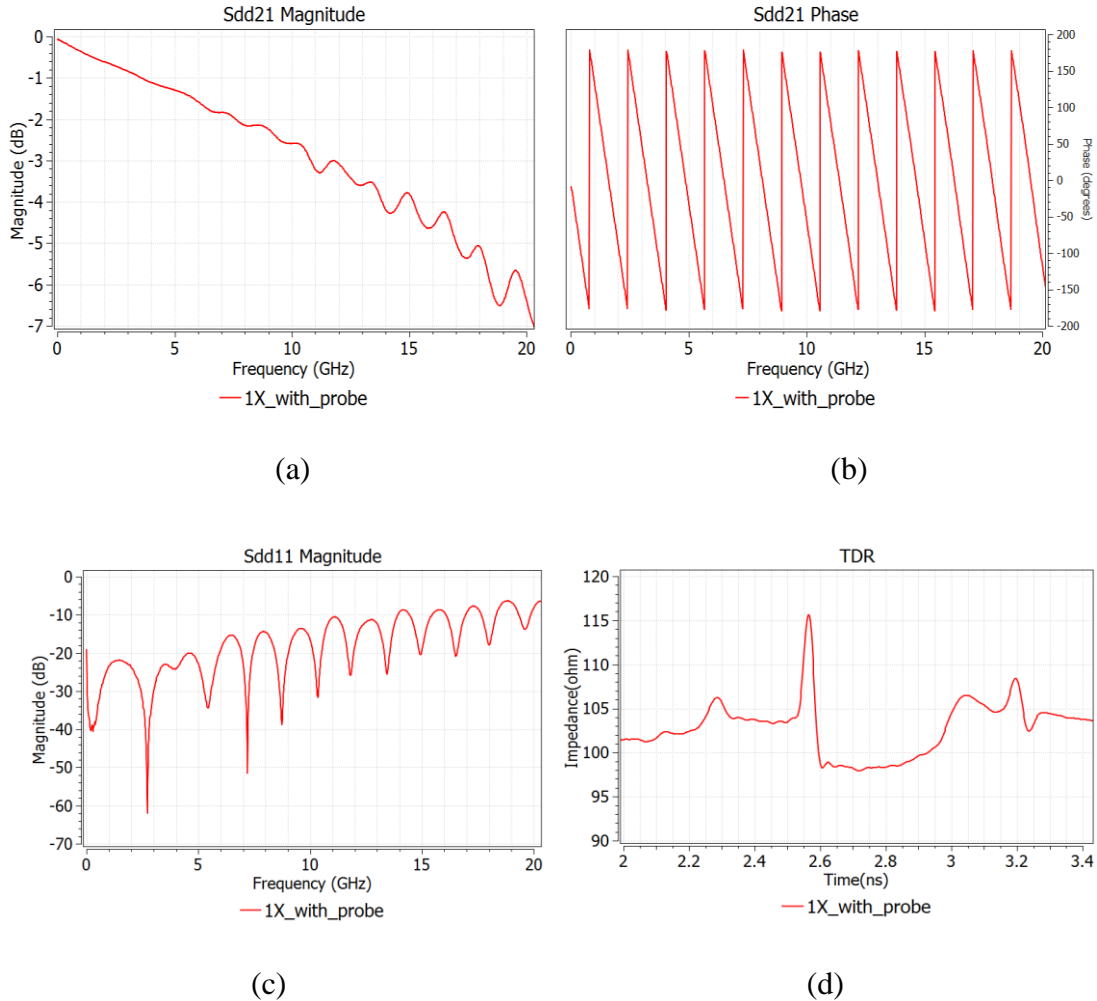
Figure 3.16. Measurement results for 1X with probe. (a) and (b) show the magnitude /phase of insertion loss; (c) shows the magnitude of return loss; (d) shows the TDR for 1X with probe also marked the delay for each parts.

Figure 3.17 shows the top view of 2X-Thru and the corresponding measurement results. In the real board, there includes the 4 edge connectors and differential traces, it is exactly the same as full wave model as discussed in the previous section. Before doing measurement, the calibration has done. And after calibration, the edge connector connected to the VNA cable. The total loss for 2X Thru on the real board is about 10dB, and return loss is less than 10dB up to 20GHz.
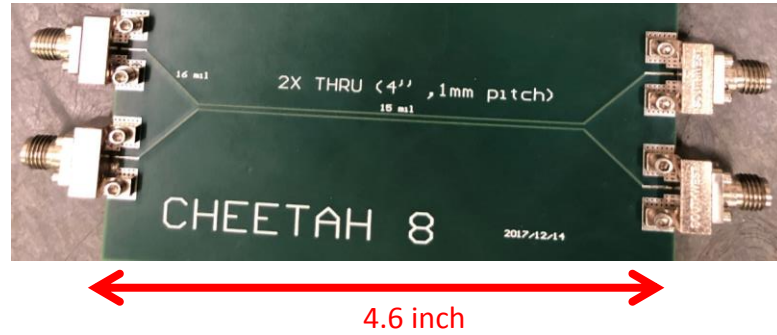
(a)
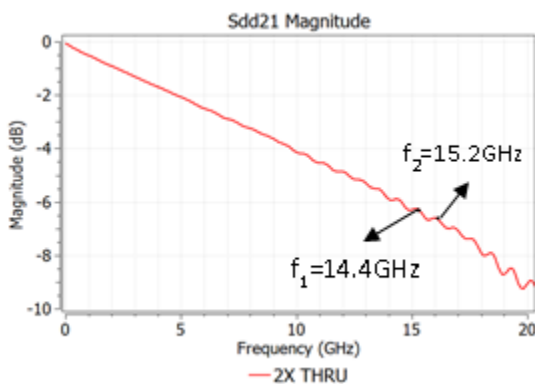
(b)
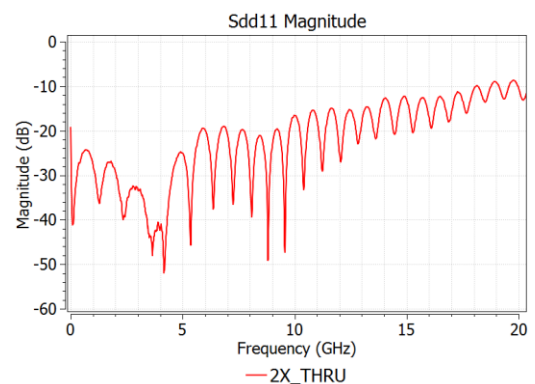
(c)

Figure 3.17. Measurement results for 2X-Thru fixture. (a) shows the top view of 2X-Thru; (b) and (c) show the magnitude of insertion loss and return loss, respectively.

3.3. PHYSICS BASED CIRCUIT MODEL FOR 1MM PITCH D PROBE

In this section, the physics based circuit will be build and the simulation results will be compared with real measurement results.

3.3.1. S Parameter of 1mm Pitch D Probe. As discussed in the previous section, the S-parameter of the D-probe can be extracted from the 2X-Thru SFD method. The physics-based model can be subsequently built in the ADS. Figure 3.18 shows the magnitude and phase of insertion loss. The total loss of the D-probe is less then 2dB up to 20GHz, indicating that the 1mm pitch D-probe exhibits good performance up to 20GHz.
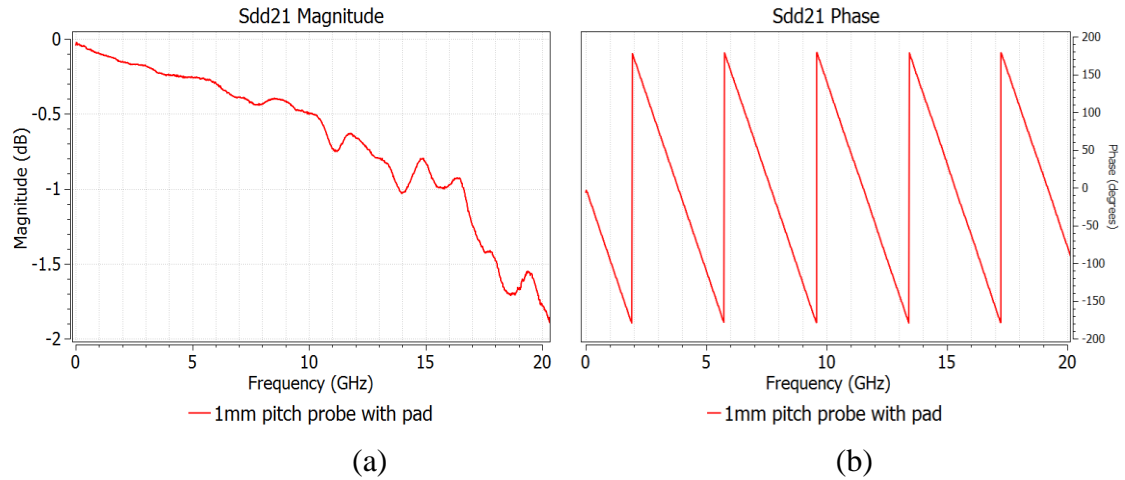
Figure 3.18. S-parameter of the 1mm pitch D-probe. (a) and (b) show the magnitudes of insertion loss and return loss.

After de-embedding, only the adaptor and D-probe remain; Figure 3.19 shows the TDR results for de-embedding. The total delay is 0.75ns, delay for the adaptor is 0.3ns, and delay for the D-probe is 0.45ns. A large bump can be observed in the TDR curve due to the inductance of probe tips.
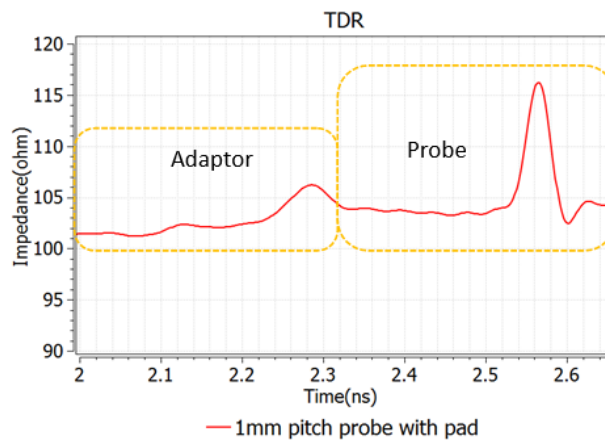
Figure 3.19. TDR result for 1mm pitch D probe.

3.3.1. Physics Based Circuit Model for 1mm Pitch D Probe. Figure 3.20(a)
shows the different mode current paths for the D-probe. Blue lines represent the electrical
current density, and pink lines represent the displacement current density. The
displacement current is a quantity appearing in Maxwell's equations and is defined in
terms of the rate of change of the electrical displacement field. It implies that a varying
magnetic field generates a varying electric field. Hence the rate of change of this current
caused by the varying electric field is the displace current. The differential current path
demonstrates the physics of operation of the D-probe. As discussed in the previous
section, the differential signal does not require GND as a reference plane; the signals can
act as a reference plane for each other [27]. Based on the current path distribution, the
one-to-one corresponding equivalent circuit model for probe tips is also shown in Figure
3.18(b). The equivalent circuit model plot includes several parts: inductance of probe tips
(L1), inductance of transom (L2), mutual inductance of probe tips, capacitance of probe
edge to U-shaped pad (C1), capacitance of probe tip to probe tip (C2), and the
capacitance of the probe tip to U-shaped pad (C3).

(a)   (b)
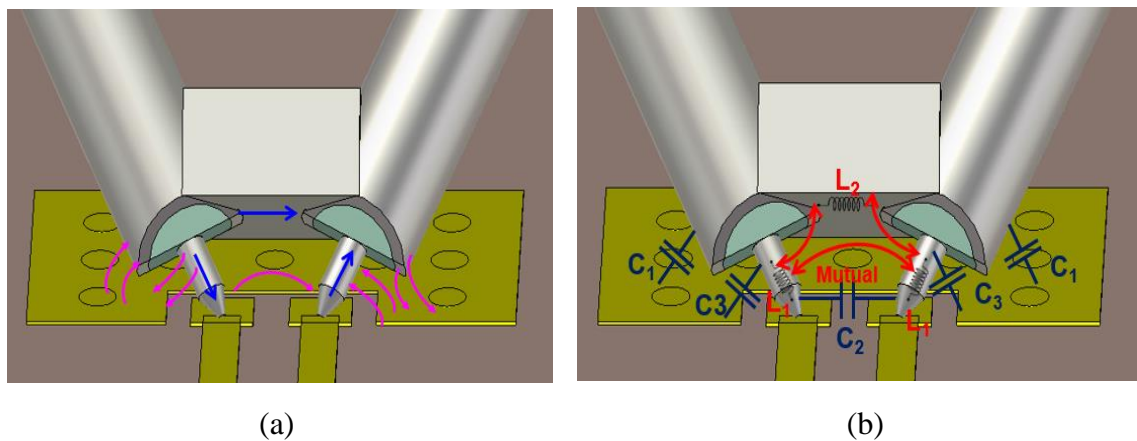
Figure 3.20. Differential mode current path and equivalent circuit model on tips.

In order to obtain the equivalent circuit model for all structures, which includes adaptors, the probe, probe tips, and U-shaped pad, further measurements are made to determine the length of the adaptor and D-probe. Figure 3.21 shows measurement of the adaptor and probe. Probe length is 1,219mil, and adaptor length is 1,093mil.

(a)   (b)
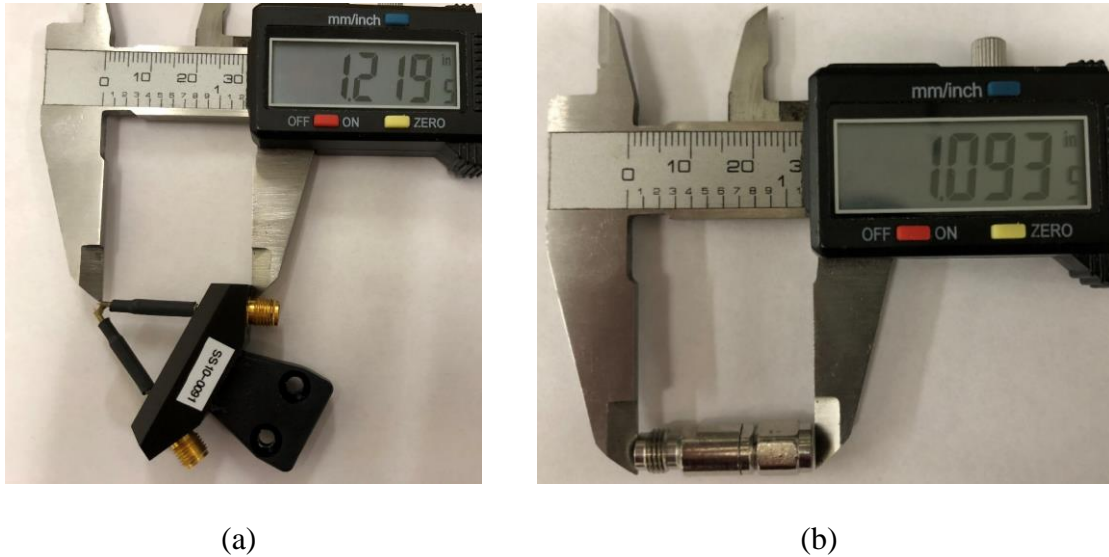
Figure 3.21. Length measurement for D probe and adaptor.

Figure 3.22 (a) shows the physics based circuit model for 1mm D probe, which simulated up to 20GHz with step 10MHz. This model include 4 parts: precision adaptors, coax, probe tips and short TL. For each part, the detailed parameters are shown in Figure 3.22 (b) to Figure 3.22 (c). Probe tips are the main part of this circuit model, which is the same as equivalent model and current path as discussed previous section. The values of probe tips are shown in the Figure 3.22 (c). The probe tips include 5 capacitors, 3 inductors and 3 mutual inductors. Because the structure of probe is symmetric, the

capacitance between two sides are the same. The mutual inductors are also the same between probe tips to center beam.
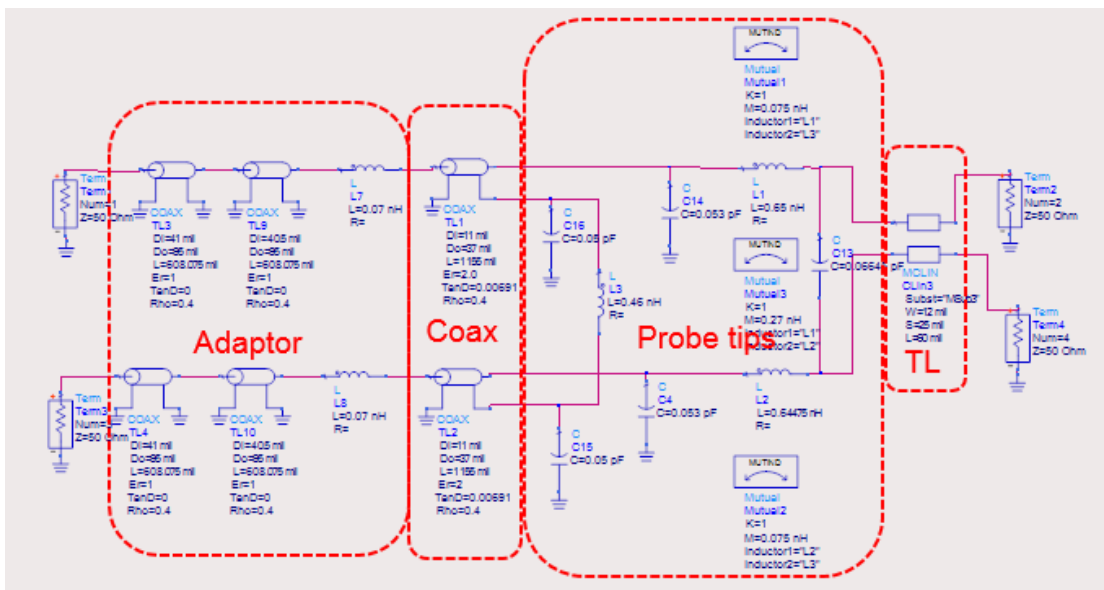
(a)
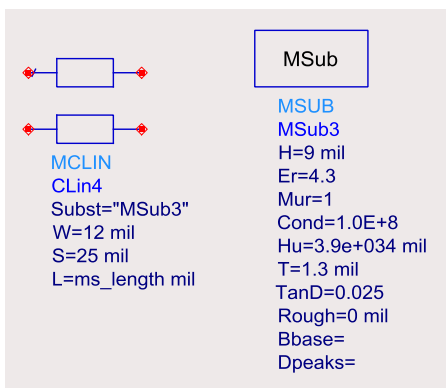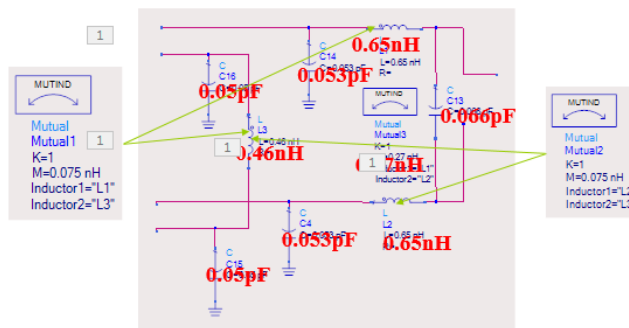
(b)   (c)

Figure 3.22. Physics-based circuit model for 1mm D probe; (b) to (c) shows the detail for probe tips and short TL, respectively.

The parameters shown in the physics-based circuit model are reasonable with minimal tuning in the model to match the measurement results. This model also matches

the current path. Comparison of the simulation result and measurement result is shown in Figure 3.23, which includes the differential mode magnitude and phase of insertion loss, and the differential mode magnitude and phase of return loss. The results show a very good match.

(a)

(b)

(c)

(d)
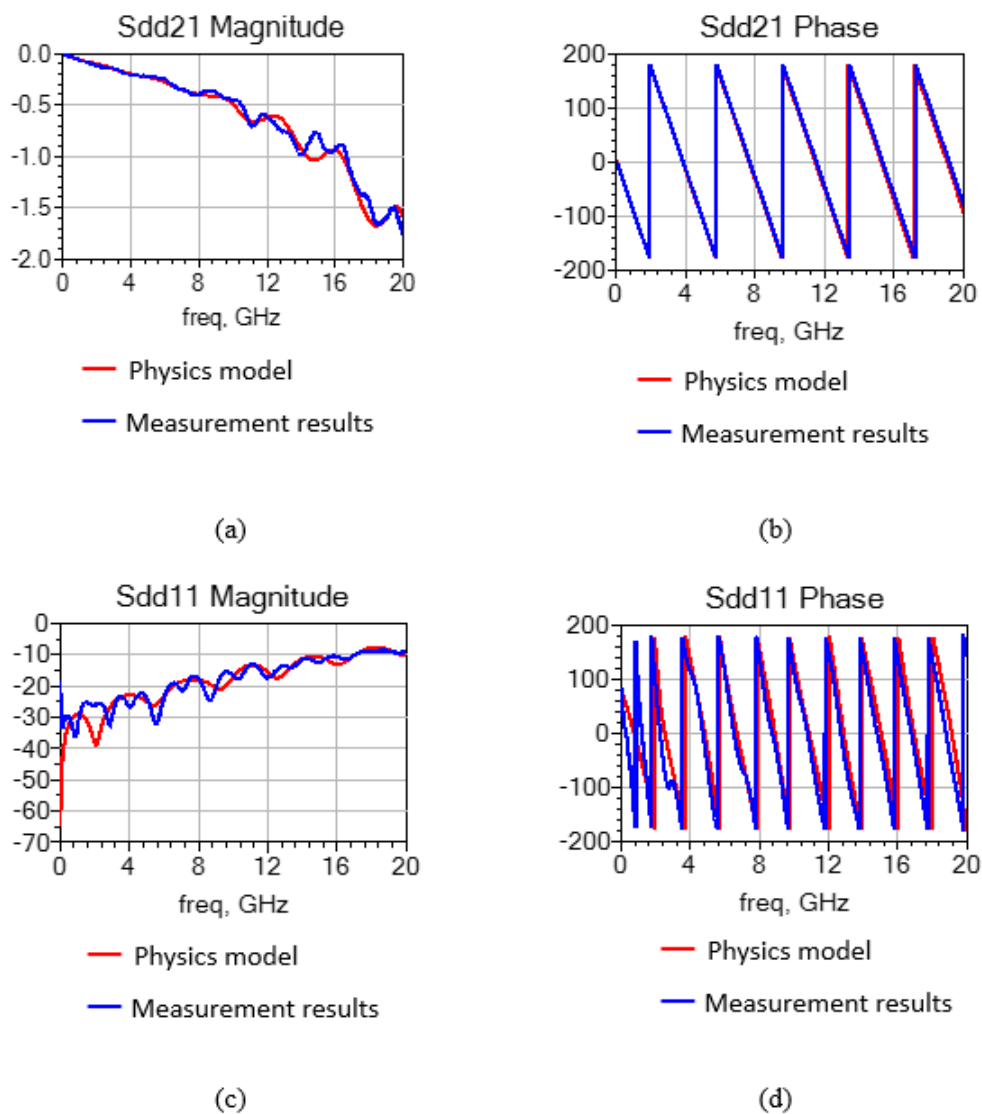
Figure 3.23. Comparison for physics based circuit model and measurement results, (a) and (b) shows magnitude and phase of insertion loss; (c) and (d) shows the magnitude and phase of return loss.

Results of the physics-based circuit model and measurement show an excellent match. Hence, this circuit model could be used in probe development. Because inductance in probe tips plays an important role, a suggestion for the next generation is to reduce the inductance or mutual inductance of the probe tip, in order to improve the performance of the probe.

3.4. TEST VEHICLE DESIGN FOR AITT DEMO

AITT is powerful software which is developed by MST EMClab. In this section, a test vehicle is designed to test the AITT software.

3.4.1. Introduction to AITT. AITT is a powerful software developed by MST EMCLAB. The four key functions of AITT are VNA control, analysis, de-embedding, and applications.

- VNA control: control of a VNA locally or remotely by a separate computer.

- Analysis: powerful tools for frequency domain, time domain and eye diagram analysis.

- De-embedding: multiport fixture de-embedding tool that supports 2X Thru and 1-port open/short techniques.

- Applications: comprehensive solutions for PCB characterization (Delta-L+, material extraction, surface roughness), and cable characterization.

Delta-L methodology is one of the key functions of AITT, and accommodates the different focuses and needs of the different stages of PCB manufacturing. Based on different cases, the Delta-L provides a different algorithm. Delta-L can thus provide accurate de-embedding with full S-parameter extraction, in addition to material extraction

capability, and allows for flexibility and the capability of HVM monitoring by a smaller coupon. Figure 3.24 outlines the various Delta-L methodologies and the most suitable cases for each. The Delta-3L method requires three traces to deliver the highest accuracy. Delta-L only needs one trace, which can be used for impedance validation and HVM monitoring. Finally, Delta-2L needs two traces, and is the most cost-effective method. This method could be suitable for board quality validation, insertion loss, and impedance validation.
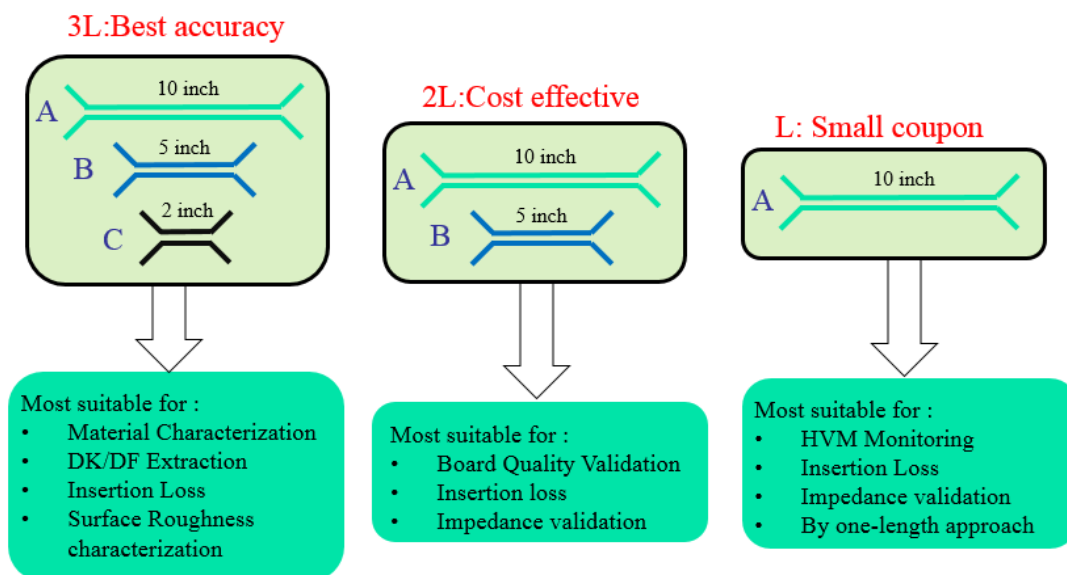
Figure 3.24. Different Delta-L methodology and most suitable cases.

3.4.2. Test Vehicle Design. In order to test AITT software functions, a test vehicle is designed to test AITT software functions. And this test vehicle is designed up to 40 GHz, which has been validated in full wave models.

The two largest parts of the boards are the 2.92mm connector parts, 1mm pitch probe, and 0.5mm pitch probe part. The material used for the board is Megtron 6, with a Dk of 3.6 and Df of 0.002 at 1GHz. The stackup details are shown in Figure 3.25. A four-

layer board is used with a total thickness of 70.27mil, and all signal traces are routed in

layer 3.

Layer №	LAYER DESCRIPTION	Segment	Cu WT(OZ PER SQ FT)	EST THK (MILS)	Single Ended (50 Ohms+/-10%)			Differential (85 Ohms+/-10%)			Dk
					TARGET LW(MILS)	FINISHED LW(MILS)	Calculat ed Zo	TARGET LW/LS (MILS)	FINISHED LW/LS (MILS)	Calculat ed Zdiff	
	SOLDERMASK										
1	PRIMARY SIDE	Cu	1.0 FINISHE	1.7	15.00	15.00	50.42				
		Prepreg	2x3313	7.87							3..88
2	GND	Cu	0.5	1.7	REF	REF	REF	REF	REF	REF	
		Core	R5775N	48.4							3.4
3	SIGNAL	Cu	0.5	1.7	10.71	10.71	50.00	11.50/11.50	11.50/11.50	85.00	
		Prepreg	2x3313	7.2							3..88
4	SECONDARY SIDE (GND)	Cu	1.5 FINISHE	1.7	REF	REF	REF	REF	REF	REF	
	SOLDERMASK										
	Est Board thickness over conductors (mils)			70.27							
	Meg6										

Figure 3.25. Stackup information for AITT demo board V2.

Figure 3.26 shows the layout review which size is 12inch*10inch. In this test vehicle design, the 2.92mm connector part is needed as a golden standard to verify SFD method results and Dk/Df extraction results. (b) shows the details for 2.92mm connector design; (c) shows the details for 1mm pitch probe pad (left) and 0.5mm pitch probe pad (right).

(a)   (b)   (c)
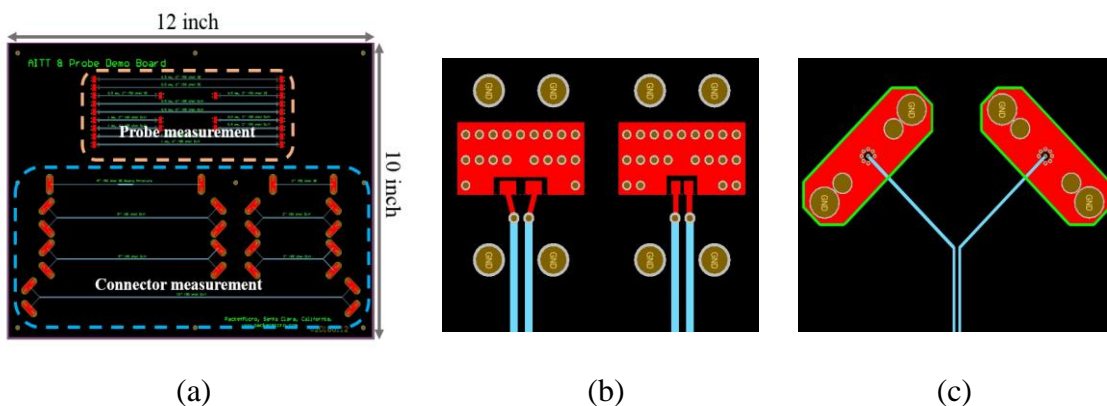
Figure 3.26. AITT board layout review;(a) probe launch pattern and 2.92mm connector test vehicle layout.(b) shows details review of 2.92 mm connector part; (c) shows details review of 1mm pitch probe pad (left) and 0.5mm pitch probe pad (right).

To ensure that the trace routing can work up to 40GHz, a full wave model has been built. The author optimized the transition from a 0.5mm pitch probe to a PCB in a high-speed signal application. The optimization includes 100ohm characteristic impedance via the design, touch pad sizing, anti-pads, and diving board effects, as well as a tear-drop shape design, in the transition from signal vias to lead-in traces.

(a)

(b)   (c)
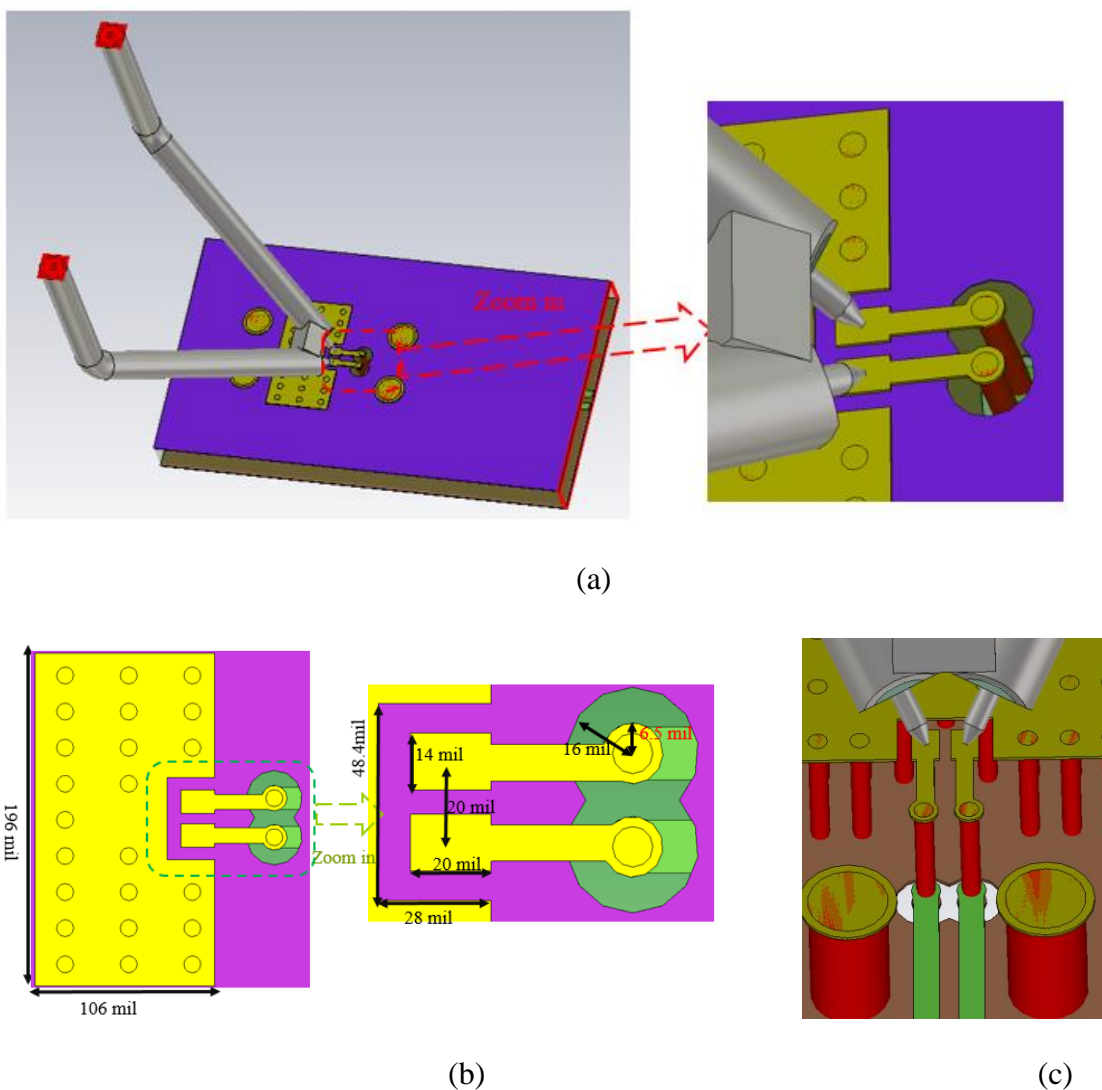
Figure 3.27. Full wave model of 0.5mm pitch probe transition to PCB.

Figure 3.27 shows the full wave model of the 0.5mm pitch probe transition to PCB. Detailed values of the probe pad are shown in Figure 3.27(b), and a side view of the probe to the signal trace on Layer 3 is shown in Figure 3.27(c). After optimization, the simulation results appear better; comparison results are shown in Figure 3.28. Figure 3.28 (a) compares the insertion loss magnitude, while (b) compares the TDR results.

(a)   (b)
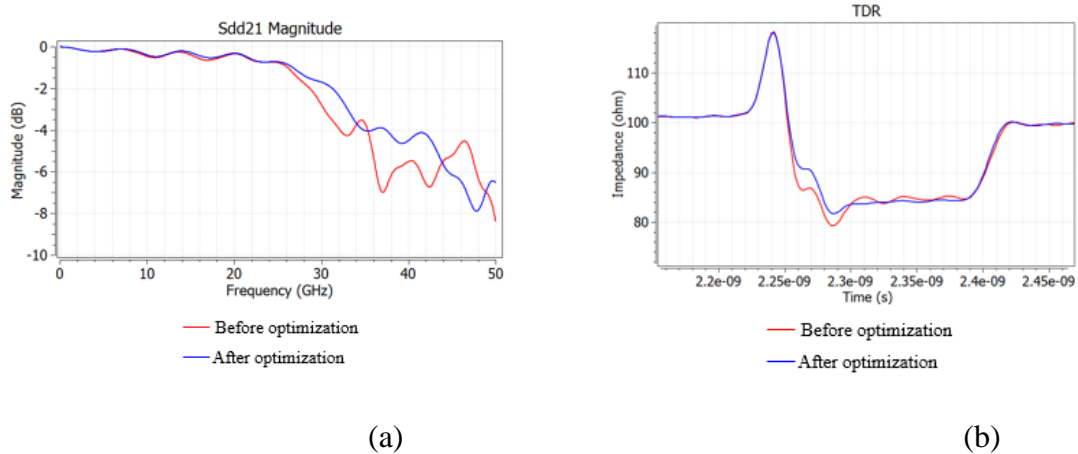
Figure 3.28. Simulation results comparison for insertion loss and TDR ;(a) Sdd21 magnitude comparison; (b) TDR result comparison.

4. CONCLUSIONS

1X-Reflect, 2X-Thru SFD, and 1-port AFR are compared, with an emphasis on calibration patterns, fixture characterization, and de-embedded results. Compared with classical calibration and de-embedding methods these three methods decrease the complexity of measurements, yet maintain their accuracy. Furthermore, simulation reveals the algorithm correctness of all the examined methods. In the manufactured test vehicle, the extracted electrical performance of a USB-C cable indicates that 1X-Reflect and 2X-Thru show a better agreement with the specification.

Moreover, a comprehensive study for a novel differential probe is provided, and an accurate simulation model for the proposed differential probe is built. The SFD method is used to extract the S-parameter of a 1mm pitch probe. A physics-based circuit model is built up to 20GHz, with corresponding one-to-one geometry features and each circuit element of the probe. This physics-based circuit could provide the guidelines for a next-generation probe. Finally, a test vehicle is built to validate functioning in AITT. In the future, more test vehicles will be designed to study surface roughness with the unified probe launch pattern.

BIBLIOGRAPHY

[1]   Bichen Chen, Xiaoning Ye, Qiaolei Huang, Shuai Jin, Jun Fan., "Thru-Line De-embedding (TLD), an Accurate and Simplified Fixture Removal Method with Self-validating Line Standard. " In *DesignCon, 2017*.

[2]   G. F. Engen and C. A. Hoer, "Thru-Reflect-Line: An Improved Technique for Calibrating the Dual Six-Port Automatic Network Analyzer," in Microwave Theory and Techniques, IEEE Transactions on, vol. 27, pp.987-993, 1979.

[3]   H. Cho and D. Burk, "A three step method for the de-embedding of high frequency S-parameter measurements." in IEEE Trans. Electron Devices, vol. 38, pp. 1371–1375, June 1991.

[4]   Bichen Chen, Xiaoning Ye, Bill Samaras,Jun Fan, "A Novel De-Embedding Method Suitable for Transmission-Line Measurement." In *IEEE Asia-Pacific Symposium on Electromagnetic Compatibility, May 25-29, 2015*.

[5]   Q. Huang, J. Li, J. Zhou, W. Wu, Y. Qi and J. Fan, "De-embedding method to accurately measure high-frequency impedance of an O-shape spring contact." In *2014 IEEE International Symposium on Electromagnetic Compatibility (EMC)*, Raleigh, NC, 2014, pp. 600-603.

[6]   Bichen Chen, Xiaoning Ye, Qiaolei Huang, Shuai Jin, Jun Fan "Thru-Line De-embedding (TLD), an Accurate and Simplified Fixture Removal Method with Self-validating Line Standard. " In *Proc. of DesignCon*, 2017.

[7]   Shuai Jin, Xiang Fang, Bichen Chen, Han Gao, Xiaoning Ye, Jun Fan., "Validating the transmission-line based material property extraction procedure including surface roughness for multilayer PCBs using simulations." In *Electromagnetic Compatibility (EMC),* 2016 IEEE International Symposium.

[8]   S. Jin, Bichen Chen, X. Fang, H. Gao and J. Fan., "Improved "Root-Omega" method for transmission-line based material property extraction for multilayer PCBs." In *IEEE Trans. On Electromagnetic Compatibility*. Vol. 59, no. 4, pp1356-1367, March 2017.

[9]   Guo, X; Shen, G; Khilkevich, V.V.; Drewniak, J. L., "Design Methodology for Behavioral Surface Roughness Model." in *Electromagnetic Compatibility (EMC),* 2016 IEEE International Symposium.

[10]   Jiao, X; He, H; Qian, W; Li, G; Shen, G; Li, X; Ding, C; White, D.; Scearce, S.; Yang Y; Pommerenke, D., "Designing a 3-D Printing-Based Channel Emulator With Printable Electromagnetic Materials," in Electromagnetic Compatibility, IEEE Transactions on , vol.57, no.4, pp.868-876, Aug. 2015.

[11]   Bichen Chen, Muqi Ouyang, Shaohui Yong, Yansheng Wang,Yadong Bai,Yan Zhou, Jun Fan., "Integrated Crosstalk Noise (ICN) Analysis among Multiple Differential BGA and Via Pairs by Using Design of Experiments (DoE) Method. " In *Electromagnetic Compatibility (EMC),* 2017 IEEE International Symposium.

[12]   B. Chen, J. Wang, Y. S. Cao, M. Ouyang, Y. Wang, S. Jin, X. Liu, X. Peng, and J. Fan, "Differential Integrated Crosstalk Noise (ICN) Mitigation in the Pin Field Area of SerDes Channel," in Proc. IEEE Symp. Electromagn. Compat. Signal Integrity, 2018, Long Beach, CA, USA, 2018, pp.

[13]   Q. Huang, F. Zhang, T. Enomoto, J. Maeshima, K. Araki and C. Hwang, "Physics-based dipole moment source reconstruction for RFI on a practical cellphone." In *IEEE Trans. Electromagn. Compat.,* vol. 59, no. 6, pp. 1693-1700, Dec. 2017.

[14]   Q. Huang, L. Li, X. Yan, B. Bae, H.Park, C.Hwang and J. Fan, "MoM based current reconstruction using near-field scanning." in *Proc. of IEEE Int. Symp. Electromagn.Compat.,* 2017, pp. 549-554.

[15]   C. Hwang and Q. Huang, "IC placement optimization for RF interference based on dipole moment sources and reciprocity." In *IEEE Asia-Pacific Electromagn. Compat. Symp.,* 2017, pp. 331-333.

[16]   Q. Huang et al., "MoM-Based Ground Current Reconstruction in RFI Application", accepted to be published in *IEEE Trans. Electromagn. Compat.*

[17]   Q. Huang et al., "Desense Prediction and Mitigation from DDR Noise Source," submitted to Proc. IEEE Electromagn. Compat. Symp., 2018.

[18]   Q. Huang, Y. Liu, L. Li, Y. Wang, C.Wu and J. Fan, " Radio Frequency Interference Estimation Using Transfer Function Based Dipole Moment Model," submitted to Proc. of IEEE Int. Symp. Electromagn.Compat., 2018.

[19]   Q. Wang, Y. Gao, J. Fan, J. Drewniak and R. Zai, "Differential probe characterization." In *2016 IEEE International Symposium on Electromagnetic Compatibility (EMC)*, Ottawa, ON, 2016, pp. 780-785.

[20]   H. Deng, Q. Wang, R. Zai, J. Hsu, X. Ye, Q. Chen, J. Drewniak, "A unified probe launch pattern for PCB materials characterization up to 40 GHz." in *Proc. of DesignCon, 2017*.

[21]   Bichen Chen, Mikheil Tsiklauri, Chunyu Wu, Shuai Jin, Jun Fan, Xiaoning Ye, Bill Samaras., "Analytical and numerical sensitivity analyses of fixtures de-embedding." in *Electromagnetic Compatibility (EMC),* 2016 IEEE International Symposium.

[22]   Chunyu Wu, Bichen Chen, Tsiklauri Mikheil, Xiaoning Ye, Jun Fan., " error bounds analysis of de-embedded results in 2x Thru de-embedding methods" in Electromagnetic Compatibility (EMC), 2017 IEEE International Symposium.

[23]   Xiaoning Ye, Jun Fan, Bichen Chen, James L. Drewniak, Qinghua Bill Chen, "Accurate characterization of pcb transmission lines for high speed interconnect." in *2015 Asia-Pacific Symposium on Electromagnetic Compatibility (APEMC)*.

[24]   G. Maghlakelidze ,X. Yan ,L. Guan, S. Marathe , Q. Huang, B. Bae , C. Hwang ,V.Khilkevich , J. Fan   , D. Pommerenke., "SNR Analysis and Optimization in Near-Field Scanning and EMI Applications." accepted to be published in *IEEE Trans. Electromagn. Compat.*

[25]   Y. Wang, S. Penugonda, Y. Zhang, J. Chen, and J. Fan, "Studying the Effect of Drilling Uncertainty on Signal Propagation through Vias." in Proc. *IEEE Symp. Electromagn. Compat. Signal Integrity*, 2015, pp.365-369, 15-21 March 2015.

[26]   Y. Zhang, Y. Wang, et al., "Estimating the via-plane capacitance for differential vias with shared-antipad based on analytical equations." in Proc. *IEEE Int. Symp. Electromagn. Compat. Signal Integrity (EMCSI),* 2017, Washington, DC, USA, 2017, pp. 272-276.

[27] J. Xu, Y. Wang, et al., "A survey on modeling strategies for high-speed differential Via between two parallel plates," in Proc. IEEE Int. *Symp. Electromagn. Compat. Signal Integrity (EMCSI),* 2017, Washington, DC, USA, 2017, pp. 527-531.

VITA

Yuan Chen was born in Hanchuan, Hubei, China. She received her B.S. degree in Electronics Commerce from Central China Normal University, Wuhan, China, in 2014. She joined the EMC Laboratory in the Missouri University of Science and Technology, Rolla, in 2015 and received a master of science degree in Electrical Engineering in May, 2018. She worked as a summer intern at Amphenol TCS in 2016 and worked as a CO-OP in Cisco hardware group. Her research interests included signal integrity in high speed digital systems, probe design, high speed PCB design, and Electromagnetic interference control.